Modeling and Analysis of Power-to-hydrogen based Alumina Hydrate Calcination for Low-carbon Aluminum Making

Ruqiya Abdullah Mohammed

M.Sc. Thesis

December 2023

A thesis submitted to Khalifa University of Science and Technology in accordance with the requirements of the degree of M.Sc. in Mechanical Engineering in the Department Mechanical and Nuclear Engineering.

Modeling and Analysis of Power-to-hydrogen based Alumina Hydrate Calcination for Low-carbon Aluminum Making

by

Ruqiya Abdullah Mohammed

A thesis submitted in partial fulfillment of the requirements for the degree of

M.Sc. in Mechanical Engineering

at

Khalifa University

Thesis Committee

Prof. Valerie Eveloy (Main Advisor)
Khalifa University
Dr. Nicolas Calvet (Co-Advisor)
Khalifa University
Dr. MD Didarul Islam (RSC Member 1)
Khalifa University
Dr. Khalid Al Ali (RSC Member 2)
Khalifa University

December 2023

Abstract

Ruqiya Abdullah Mohammed, "**Modeling and analysis of power-to-hydrogen based alumina hydrate calcination for low-carbon aluminum making**", M.Sc. Thesis, M.Sc. in Mechanical Engineering, Department Mechanical and Nuclear Engineering, Khalifa University of Science and Technology, United Arab Emirates, December 2023.

The aluminum industry is a highly energy-intensive sector with high-temperature processes currently mainly driven by fossil fuels. The demand, production, and use of aluminum are increasing and so are the emissions. It is estimated that the aluminum industry consumes 95 MJ of energy and emits 11.5 tons of carbon dioxide (CO_2) per ton of aluminum produced, resulting in 0.45-0.5 Gt of global CO_2 equivalent emissions annually. Alumina smelting and refining aluminum are responsible for over 90% of aluminum production's direct CO_2 emissions, the rest being from recycled production, anode production, and casting. Although aluminum smelting is the most energy-intensive process step, the energy input is essentially electricity and can therefore be decarbonized. However, the Bayer process where alumina is produced from bauxite is thermal energy intensive due to the calcination step carried at up to 1100 °C, which is dependent on the use of fossil fuels. Climate change targets call for the development of smart strategies and technologies for not only decarbonizing electricity generation, but also heat supply. One of the most promising technologies to switch from fossil fuels in high-temperature industrial processes is power-to-gas (PtG). This process also provides the possibility to store surplus energy from intermittent energy sources in the form of hydrogen or synthetic natural gas. Since hydrogen combustion produces no carbon emissions, power-to-hydrogen (PtH_2) is a potential solution to significantly reduce alumina hydroxide calcination emissions depending on technical, cost, and retrofit considerations.

The objective of this Thesis is to reduce greenhouse gas (GHG) emissions in the calcination process through the use of PtH_2 in place of conventional fuels. This is achieved using process modeling to evaluate the energy consumption and emissions of PtH_2-based calcination in comparison with natural gas-based calcination. Steady-state mass and energy conservation are applied to each system component. The thermodynamic model is validated by comparison of stream properties and overall energy consumption and emissions with reference data for a conventional natural gas-based calcination process. The energy consumption and emissions of the low-carbon hydrogen-based process are compared with that of the conventional natural gas-based calcination process.

The energy consumption of the low-carbon hydrogen-based calcination process, 2.8068 GJ per ton of alumina (equivalent to 5.3462 GJ per ton of aluminum), excluding water electrolysis for hydrogen production, is similar to that of the conventional process under the modeling assumptions made. In parallel, at an electricity emission factor of for example 10 gCO_2 per kWh_e, calcination emissions are almost eliminated (i.e., reduced by 0.1554 tCO_2 per ton of alumina, equivalent to 0.296 tCO_2 per ton of aluminum (13.8% of total conventional system emissions).

Sensitivity analysis reveals that alumina calcination energy consumption for both the conventional and hydrogen-based process is influenced by the efficiency of the alumina direct cooling stages. The total emissions from the low-carbon hydrogen system are primarily sensitive to the electricity emission factor. At an electricity emission factor of 40 gCO_2 per kWh or lower, the H_2-based calciner and aluminum smelting systems have lower emissions than the conventional system.

Indexing Terms: Aluminum, calcination, industrial decarbonization, hydrogen.

Acknowledgement

First and foremost, I would like to extend my sincere gratitude and appreciation to Dr. Valerie Eveloy. Her unwavering support throughout this project has been invaluable. Dr. Valerie was always available when I needed assistance, and I greatly benefited from her extensive knowledge and guidance, which were instrumental in the successful completion of this study. I would also like to express gratitude to Dr. Nicolas Calvet for his encouragement and interest.

I am also grateful to Ph.D. student Hammad Masood, and M.Sc. student Sajeer Ahmed for their contributions to improving the aluminum production process model. I'm equally thankful for the valuable suggestions provided by Dr. Pravin Kannan.

I would like to acknowledge the steadfast support of my friend, Alia. Her presence throughout this journey, along with her constant encouragement, played a pivotal role in motivating me to do my best in completing this thesis.

Finally, I want to express my deepest gratitude to my family for their unwavering support during these two years.

The Thesis research was supported by Khalifa University research grant CIRA-2020-080.

Dedication

This thesis is proudly dedicated to my late mother *Fatima Ibrahim* who loved me unconditionally and surrounded my life with her love, care, support, and prayers.

Although it was a tough journey without you, your warm smile has been a source of motivation and strength during moments of despair and discouragement.

This thesis is also dedicated to my father *Abdullah Farah* who made sacrifices so I would have access to high-quality education from an early age.

Declaration and Copyright

Declaration

I declare that the work in this thesis was carried out in accordance with the regulations of Khalifa University of Science and Technology. The work is entirely my own except where indicated by special reference in the text. Any views expressed in the thesis are those of the author and in no way represent those of Khalifa University of Science and Technology. No part of the thesis has been presented to any other university for any degree.

Author Name: Ruqiya Abdullah Mohammed _____

Author Signature: 

Date: 15/12/2023_____

Copyright ©

No part of this thesis may be reproduced, stored in a retrieval system, or transmitted, in any form or by any means, electronic, mechanical, photocopying, recording, scanning or otherwise, without prior written permission of the author. The thesis may be made available for consultation in Khalifa University of Science and Technology Library and for inter-library lending for use in another library and may be copied in full or in part for any bona fide library or research worker, on the understanding that users are made aware of their obligations under copyright, i.e. that no quotation and no information derived from it may be published without the author's prior consent.

Contents

Abstract I
Acknowledgement II
Dedication III
Declaration and Copyright IV
List of Figures VI
List of Tables VII
Nomenclature VIII
1. Introduction 1
2. Literature Survey 3
2.1 Aluminum Production Process 3
2.2Aluminum Industry Decarbonization 7
2.2.1 Decarbonization of the power supply 8
2.2.2 Decarbonization of process emissions 9
2.2.3 Increased scrap recycling 10
2.3Power-to-Gas 11
2.4 Summary 12
3. Thesis Aim, Scope, Approach, Tasks and Expected Outcomes 13
3.1Overall Aim 13
3.2Scope and Approach 13
3.2.1 Alumina refining process and PtG process configurations 13
3.2.2 Energy sources for power-to-hydrogen and alumina electrolysis 13
3.2.3 Scheme thermodynamic, and environmental performance assessment 13
3.2.4 Modeling approach 14
3.3Work Packages 14
3.4 Expected Outcomes and Deliverables 14
4. Power-to-Hydrogen Alumina Hydrate Calcination Scheme 15
5. Modeling and Analysis Methodology 18
5.1Analyses 19
5.1.1 CFB calciner 19
5.1.1.1 Preheating stages 19
5.1.1.2 Cooling stages 21
5.2Thermodynamic Process Model 24
5.2.1 Calciner specific energy consumption calculation 27
5.2.2 Hall-Heroult process 30
6. Results and Discussion 32
6.1Comparison of Modeling Results with Literature Values for the Conventional Calcination and Smelting Process 32
6.2Comparison of Energy Consumption and Emissions for the Conventional and PtH_2-based Processes 33
6.3Emissions in different Countries 34
6.4Sensitivity Analysis 36
7. Conclusions and Recommendations 39
7.1Conclusions 39
7.2Recommendations 39
8. References 40
Appendix I 47

List of Figures

Number	Title	Page
1	Schematic diagram of the overall aluminum production process, based on [29].	4
2	Schematic process flow diagram of the Bayer process for alumina refining, based on [30].	5
3	Phase changes during calcination of hydrate [111].	6
4	Change in installed cost, capacity factor and LCOE of renewable sources (2010–2021) [32].	9
5	PtH_2 concept, including hydrogen end-use applications [49].	12
6	Schematic of the Hydrogen calciner furnace coupled with an aluminum smelting process (electrolysis). LTE electrolyser is considered for hydrogen production.	16
7	Schematic of the conventional calciner furnace fueled by natural gas coupled with an aluminum smelting process (aluminum electrolysis).	17
8	Progressive drop in specific energy consumption versus calciner technology [100].	19
9	Outotec-circulating fluid bed calciner flowsheet [23].	20
10	Conceptual fluid bed cooler with the hot-end section (primary air heating), and cold-end section (final alumina product cooling). Also, the expected solids temperatures between the different stages are indicated, re-drawn based on [22].	21
11	Calcination of alumina hydrate process	27
12	Aluminum reduction in the Hall–Heroult process. The output products are assumed to have the same temperature as the reduction temperature of 950°C.	30
13	Carbon intensity of the PtH_2 calcination-electrolysis model in different selected countries. (Note electricity emission factors for year 2020: 0.4041, 0.5059, 0.5374, 0.33866, 0.00567, 0.00762 $kgCO_2/kWh$) for UAE, Saudi Arabia, China, Germany, Sweden, and Norway respectively). These countries are responsible for 3.83%, 1.53%, 57.15%, 2.75%, 0.2%, and 2% of global aluminum production in year 2020. Emissions represented are indirect emissions from electricity usage of each air blowers/ESP, H_2 production, and smelting, in addition to direct emission of anode consumption and anode baking.	35
14	Sensitivity analysis to identify the parameters that influence the specific energy requirements of the calciner.	37
15	Sensitivity analysis to identify the key parameters that have the most significant impact on the CO_2 emissions generated by the PtH_2 calcination-electrolysis systems.	37
16	Parametric analysis to study the effect of emission factor on the total emissions of both the NG- and the H_2-based calcination-electrolysis systems.	38

List of Tables

Number	Title	Page
1	Energy consumption per ton of sawn aluminum ingot production.	6
2	Engineering and process improvement technologies that result in direct emissions reductions in the aluminum industry.	7
3	Input modeling parameters calcination-alumina electrolysis.	25
4	Prediction discrepancy between the present model and thermodynamic property tables for NG-based calcination and aluminum smelting processes.	26
5	Prediction discrepancy between the present model and thermodynamic property tables for PtH_2-based calcination and aluminum smelting processes.	27
6	Comparison of present conventional process model predictions with corresponding reference data.	33
7	Main technical energy and emission intensity modeling results for the overall calciner and alumina electrolyser processes, including calcination furnace fuel input/production, calciner air blowers and ESP, smelting electricity, smelter anode baking, anodic carbon consumed in smelting, and Al ingot casting (considered as fuel) at base case operating conditions. Ingot casting emissions are not included. Digestion, clarification, and precipitation (GJ/tAl) energy requirement (16.65[76]) and emissions are not included.	34
A1	Coefficients of Shomate Equation for each substance in given temperature range.	40

Nomenclature

Abbreviation	Description
Al	aluminum
$Al_2O_3 \cdot H_2O$	alumina hydrate
Al_2O_3	aluminum oxide (alumina)
BAT	best available technique
CCUS	carbon capture, utilization, and storage
CFB	circulating fluid bed
tCO_2	ton of carbon dioxide
tAl	ton of liquid aluminum
tAla	ton of alumina
CSP	concentrated solar power
DHT	direct heat transfer
EEA	European Aluminum Association
ESP	electrostatic precipitator
GHG	greenhouse gas
IAI	International Aluminum Institute
LTE	low-temperature electrolyser
LPG	liquefied petroleum gas
NG	natural gas
PtG	power-to-gas
PtH_2	power-to-hydrogen
PV	solar photovoltaic
SEC	specific energy consumption
SMR	steam methane reforming
SNG	synthetic natural gas
kg	kilogram
MJ	megajoule
GJ	gigajoule
kWh	kilowatt hour
MWh	megawatt hour

Symbols

$M_{3,d,h}$	mass of dry hydrate entering the calciner after preheating stages (ton/tAl)
M_w	mass of water content in the hydrate (ton/tAl)
$M_{4,ala}$	mass of hot alumina produced (ton/tAl)
$M_{7,ala}$	mass of alumina exciting the FBC (ton/tAl)
$M_{8,Al}$	mass of liquid aluminum produced (ton/tAl)
$M_{9,C}$	mass of carbon anode (ton/tAl)
M_{10,CO_2}	mass of carbon dioxide exciting the aluminum smelter (ton/tAl)
$M_{11,w}$	mass of cooling water (ton/tAl)
$\dot{m}_{pri,a}$	mass flow rate of primary air (ton/s)
$M_{15,p,a}$	mass of primary air (ton/tAl)
$M_{18,s,a}$	mass of secondary air (ton/tAl)
$M_{19,g}$	mass of total exhaust gases (ton/tAl)
M_{22,CH_4}	mass of methane fuel (ton/tAl)

M_{22,H_2}	mass of hydrogen fuel (ton/tAl)
$T_{1,h}$	inlet hydrate temperature to the preheating stage (°C or K)
$T_{3,d,h}$	dry hydrate temperature after preheating (°C or K)
$T_{4,ala}$	hot alumina temperature after calcination process (°C or K)
$T_{6,ala}$	theoretical alumina inlet temperature to the fluid bed cooler (°C or K)
$T_{11,w}$	inlet temperature of the cooling water to the FBC (°C or K)
$T_{14,w}$	outlet temperature of the cooling water from FBC (°C or K)
$T_{13,p,a}$	outlet temperature of primary air from the FBC (°C or K)
$T_{15,p,a}$	inlet temperature of primary air to the calciner (°C or K)
$T_{16,s,a}$	inlet temperature of secondary air to the cooling stage (°C or K)
$T_{18,s,a}$	temperature of preheated secondary air (°C or K)
$T_{19,g}$	outlet temperature of hot gases exciting the calciner (°C or K)
$T_{21,g}$	temperature of waste gases exiting preheating zone (°C or K)
$\eta_{p,h}$	theoretical thermal efficiency of preheating stages (%)
η_c	theoretical thermal efficiency of cooling stages (%)
φ	heat capacity flow ratio between gases and solids (1)
$C_{p,w}$	specific heat capacity of water (kJ/kg·K)
$C_{p,ala}$	specific heat capacity of alumina (kJ/kg·K)
$C_{p,air}$	specific heat capacity of primary air (kJ/kg·K)
$Q_{FBC,h,e}$	theoretical heat loss from alumina to the air (MJ/tAl)
$Q_{FBC,c,e}$	theoretical heat loss from alumina to the cooling water (MJ/tAl)
Q_{FBC}	total theoretical heat loss to the fluid bed cooler (MJ/tAl)
$\epsilon_{FBC,h,e}$	effectiveness of the fluid bed-cooler hot-end section (%)
$\epsilon_{FBC,c,e}$	effectiveness of the fluid bed-cooler cold-end section (%)
v_{min}	minimum fluidization velocity (m/s)
g	gravitational acceleration (9.81 m/s^2)
A	calciner furnace cross sectional area (m^2)
d_p	calciner particle diameter (μm)
ρ_p	hydrate particle density (kg/m^3)
ρ_f	fluid (air) density (kg/m^3)
μ_f	fluid (air) dynamic viscosity (kg/m·s)
Ar	Archimedes number (-)
Re	Reynolds number (-)
V_{cell}	total voltage aluminum cell (V)
CE	current efficiency of aluminum cell (%)
$\eta_{Hall-Hauralt}$	Hall-Heroult process efficiency (%)
η_{LTE}	water electrolyser efficiency (%)
SEC_{cal}	specific energy consumption of calciner (GJ/tAl) or (GJ/tAla)
$SEC_{Al,elect}$	specific energy consumption of aluminum electrolyser (GJ/tAl)
SEC_{LTE}	specific energy consumption of LTE (GJ/tAl)

1. Introduction

The current rise in global greenhouse gas emissions should be reversed to prevent climate change and global temperatures from exceeding the 2°C target. The climate goal of the Paris Agreement, which is a legally binding global climate change treaty, its goal is to limit the increase in the global average temperature to well below 2°C above pre-industrial levels and to follow efforts to limit the temperature to 1.5°C above pre-industrial levels [1]. In addition, the European Union Renewable Energy Directive has set a target of more than 32% of full power generation from renewable energy by 2030, and 100% by 2050 [2]. Global demand has increased and is predicted to continue to increase in the coming century due to increases in population, affluence, and associated consumption throughout the last century, as well as increased tendencies of urbanization and electrification (among other causes) [3]. Furthermore, material production, notably bulk metals, and construction materials, contribute significantly to world energy consumption and GHG emissions [4][5]. 33% of the worldwide industrial sector is responsible for GHG emissions from 26% of primary energy consumption [6][7]. Conscious use of clean resources should be at the forefront of sustainable plant design in the future. After steel, aluminum is the most often produced metal, as well as the most commonly produced non-ferrous metal. It is manufactured on a larger scale than all other non-ferrous metals combined [8][9]. This Thesis proposal is concerned with the decarbonization of emissions-intensive aluminum-making processes, focusing on low-carbon fuel production using power-to-gas and utilization.

Aluminum is being utilized to supplant steel components, especially in the aerospace and automotive industries. It is accounted for every kilogram of aluminum that replaces mild steel, high strength steel, and cast iron avoiding 13-20 kg of GHG emissions [10]. The vital advantages of aluminum to modern society emerge from its lightweight and high strength to weight proportion and extraordinary adaptability for effective formability into complex shapes utilizing modern design features. It is likewise strong and infinitely recyclable. The many uses of aluminum can be followed by its adaptable properties. Nowadays, aluminum has one of the quickest developing demands among metals in the world. In particular, the demand is driven by a transport sector that requirements to further development of fuel efficiency and decreased energy use and emissions through lighter vehicles, trucks, and trains. Furthermore, aluminum is a key to zero-energy structures, solar applications, and packaging that conserves food and beverages and requires less energy to transport [11]. Thus, aluminum is used broadly in the

modern world and has a variety of purposes. It has boundless areas of application and has made a vast contribution to the quality of life.

However, the production of primary aluminum is one of the most energy-intensive and GHG emissions industrial processes as reported by Kermeli et al. [12]. The GHG emissions per unit of primary aluminum output are about 12.4 times and 2.3 times that of steel and copper, respectively [13]. The aluminum industry is a highly energy-intensive process, and it utilizes raised temperatures all through with an environmental impact at some stages. It is estimated that the aluminum industry produces 0.45-0.5 Gt of carbon dioxide (CO_2) equivalent emissions each year [14][15], which is answerable for 1% of anthropogenic GHG emissions [16] and 2.5% of CO_2 emissions [17]. The total world production of primary aluminum was 64.3 million metric tons in 2018, as indicated by World Aluminum [17]; of which China contributed 57%. Also, as indicated by the International Aluminum Institute (IAI), over 30 million tons of worldwide aluminum scrap is recycled yearly, ensuring its status as one of the most recycled materials on earth [18]. IAI presented aluminum sector GHG pathways to 2050 that would see a need to expand the annual primary aluminum production over the following years to as much as 90 million tons [19]. This implies an increment of around 40 % of aluminum from 2018 to 2050. Contrasted and the present worldwide average values, the annual emissions would then increase by around 400 million tons of CO_2 equivalents. Such an expansion in emissions may not be agreeable to the world public in 2040, and thus, arrangements empowering a shift to power production from only low-emission sources ought to be developed to achieve this increase. The main objective is to improve the environmental competitiveness of the aluminum industry by using low-carbon hydrogen produced from power to gas and grid-driven alumina electrolysis through low-cost solar electricity integration.

2. Literature Survey

This chapter will provide an understanding of the production processes of aluminum and recent aluminum decarbonization pathways. It is limited to the production of aluminum oxide (alumina), and the most common production processes for processing of aluminum. Mining of bauxite is not included in the review.

2.1 Aluminum Production Process

A typical aluminum production process is represented in Fig. 1. Unlike other metals, aluminum does not occur in nature. Instead, it is found in a combination of oxides and forms that are chemically very stable. Bauxite is the name given to ores with higher than 35% concentrations of aluminum hydroxide minerals. It serves as the primary ingredient in practically all alumina manufacture. Bauxites are plentiful in a number of countries such as Australia, Brazil, Guinea, Guyana, India, Jamaica, Surinam, and Venezuela. Recent discoveries of bauxite have been found in Cambodia, Saudi Arabia, and Vietnam [20]. Based on the crystalline structure and the quantity of hydrated water molecules, bauxite may be found in three primary types. Gibbsite, boehmite, and diaspore are the three types of structures. Bauxite ore is extracted and refined through the Bayer process (Fig. 2), where it is washed with a hot solution of sodium hydroxide at 110–270 °C, dissolving alumina hydrate.

Hydrated alumina is more correctly termed "aluminum hydroxide" where the water is not fixed within the crystal structure, as is the case with other hydrates; instead, it exists in the form of hydroxide radicals, releasing water upon heating. The undissolved components of bauxite can be filtered out as solid impurities (red mud). Then, the hydroxide solution is cooled, and the aluminum hydroxide is then heated by fuel combustion to 950-1100 °C mainly oil and/or NG, which breaks down into alumina giving off water vapor in the calcination process. Alumina is the feedstock in aluminum electrolysis cells with molten cryolite (Na_3AlF_6) in the Hall-Héroult process. The presence of cryolite helps to decrease the melting point of the alumina while accelerating electrolysis. In the operation of the cell, the oxygen from the alumina is then combined with carbon anode to produce CO_2, while the aluminum is placed on the cathode. Besides alumina, carbon anodes are produced by baking a mixture of hard calcined materials such as petroleum coke, coal tar pitch, and recycled anode butts at 1150°C, most often in an on-site anode plant, but some smelters obtain carbon anodes externally [21].

The primary aluminum ingot production process involves various steps, such as bauxite mining, alumina refining, carbon anode production, electrolysis, and ingot casting. To produce

1 ton of aluminum from alumina by electrolysis, the following approximate amounts of raw materials, 2.0 tons of smelter-grade alumina (Al_2O_3) from dry scrubbers are needed. According to the European Aluminum Association (EAA), in 2013, the production of one metric ton of primary aluminum required approximately 37 GJ of thermal energy and 58 GJ of electricity (Table 1). The specific energy required for the alumina refining is about 10 GJ of thermal energy and 0.65 GJ of electricity since the two major steps in alumina production are digestion and calcination, both of which use process heat. 25% of the energy used in the Bayer Process is used during the calcination process.

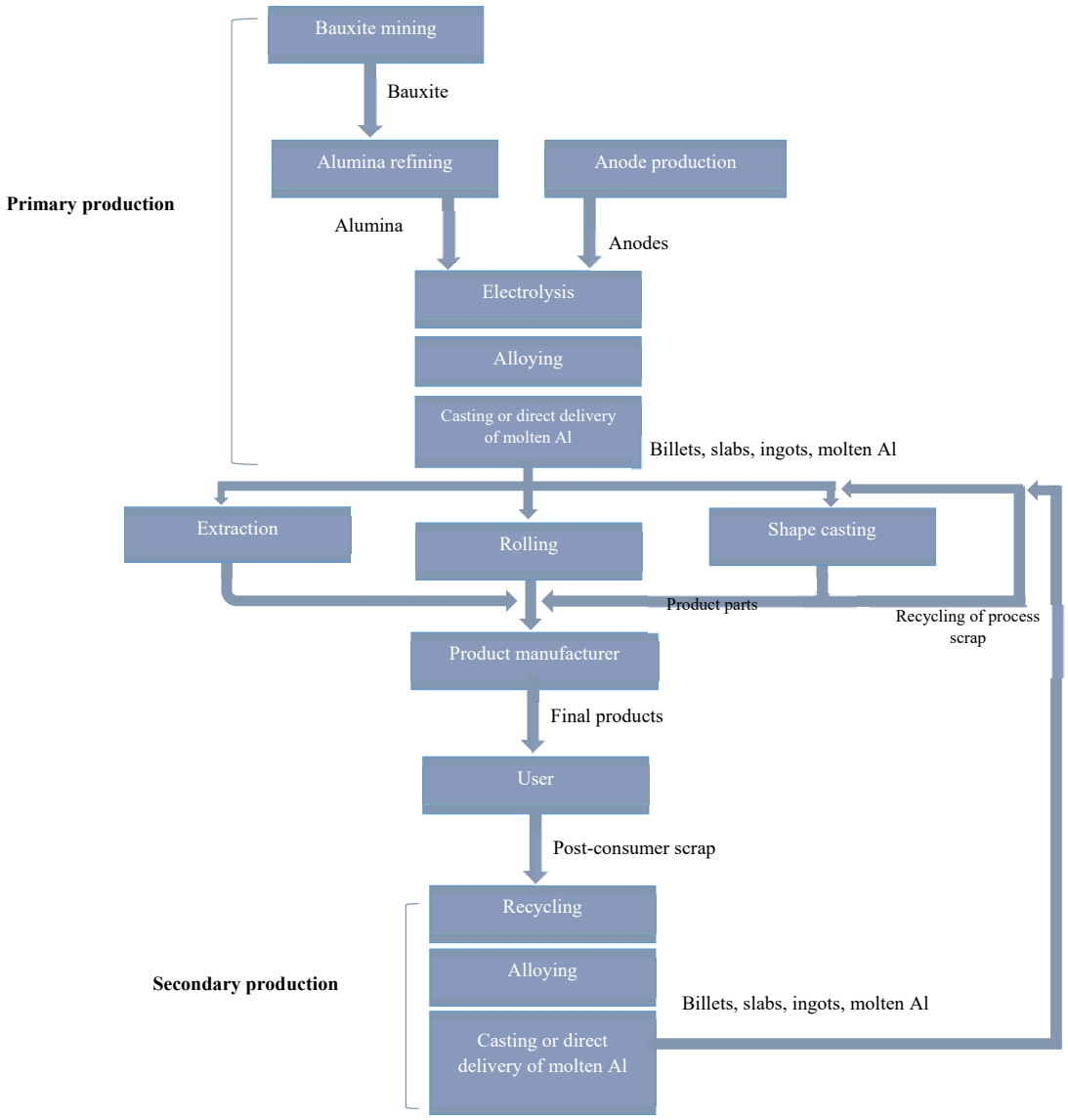


Fig. 1 Schematic diagram of the overall aluminum production process, based on [29].

The main three calcining technologies used today are rotary kilns, circulating fluidized beds (CFBs) and gas suspension furnaces. Industry has been switching from rotary kilns to stationary calciners since the oil crisis of the 1970s, with the resulting increase in the cost of fuels. Moreover, they use 3.0 GJ/t of energy instead of 4.5 GJ/t of alumina which results in 33% less energy overall [20]. CFB calciners are commonly used for producing a more uniform product and reducing energy consumption with great energy efficiency, up to 95% [22] and another study is up to 92% [23]. A gas suspension calciner is another type of calciner, unlike the circulating fluid-bed, this type has a single pass operation with a low velocity [24].

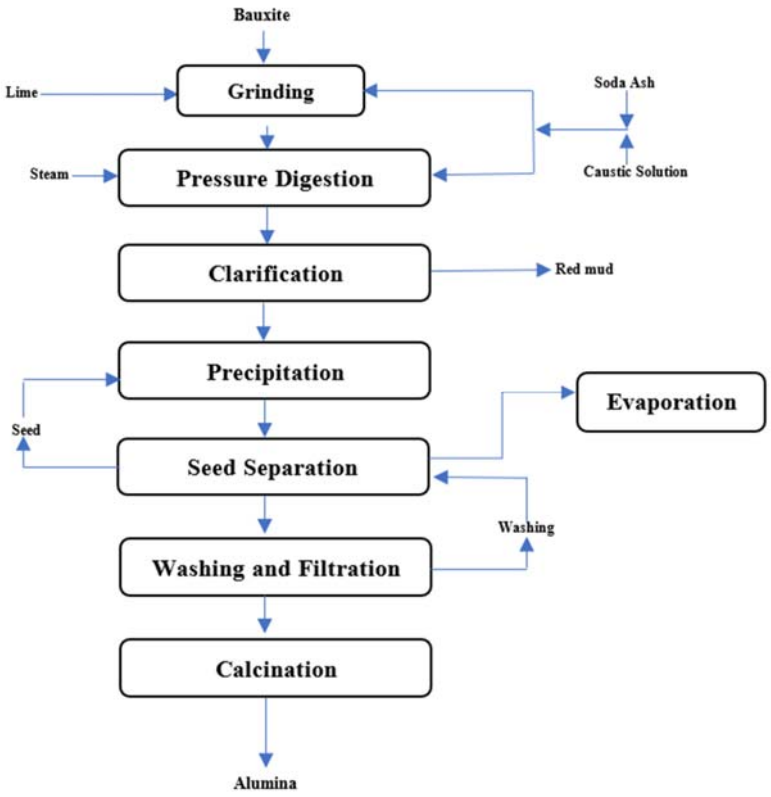


Fig. 2 Schematic process flow diagram of the Bayer process for alumina refining, based on [30].

Transition reactions in alumina phases that occur during the calcination of gibbsite and boehmite have been observed to be impacted by various factors, including temperature, heating rate, particle size, impurities, and atmospheric conditions, some of which have direct relevance to Bayer operations [111]. Figure 3 provides an overview of potential reaction pathways for gibbsite dehydration, essentially based on laboratory calcination studies [111]. In addition, the release of water vapour from combustion and calcination reactions alters water vapor pressure, which can change the reaction pathways that lead to dehydration and phase transformation

[111]. In addition, at elevated temperatures, the pressure inside a particle can cause it to fracture under flash calcination conditions [99].

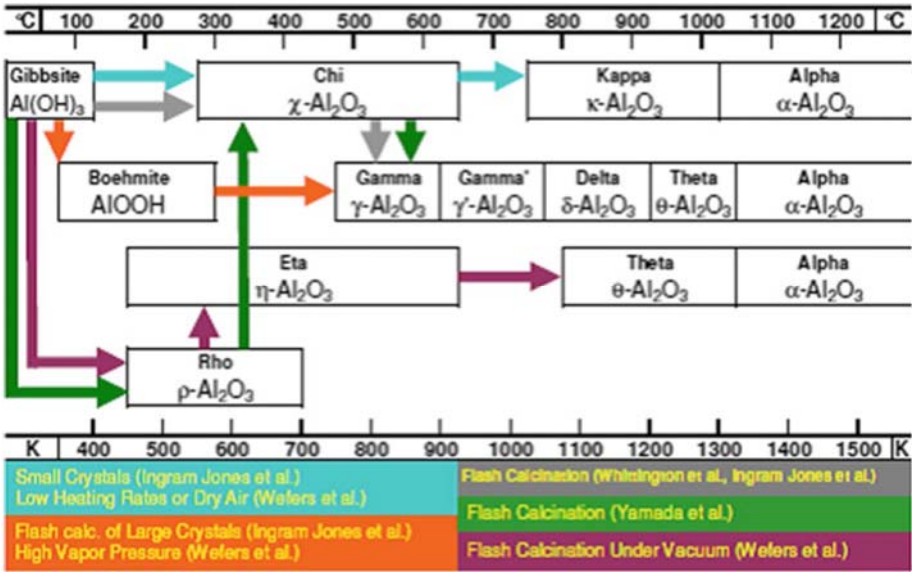


Fig. 3 Phase changes during calcination of alumina hydrate [111].

On the other hand, electrolysis is the most energy-intensive process in the aluminum cycle, consuming approximately 55 GJ (15.27 MWh) of electrical energy per metric ton of aluminum compared with the theoretical minimum energy consumption of 6.42 kWh/kg Al for cells operating at 95% current efficiency. Due to significant heat losses, the actual energy efficiency of industrial aluminum cells is only approximately 50% [20]. Based on the Alcoa Deschambault Quebec smelter, sidewall losses from the 264 reduction cells account for the majority of heat losses (up to 45% of the energy intake) [26], while exhaust gases result in energy input losses of up to 1% [25].

Table 1 Energy consumption per tonne of sawn aluminum ingot production [31].

Process	**Relative amount of product used (ton)**	**Specific energy requirement (GJ/t product)**		**Total energy requirement (GJ)**		
		Thermal Energy	Electricity	Thermal Energy	Electricity	Total
Bauxite mining	4.5	0.02	0.003	0.089	0.013	0.10
Alumina refining	1.9	10	0.65	19	1.3	21
Anode production	0.56	2.8	0.4	1.6	0.22	1.8
Electrolysis	1.0	14(*)	55	14(*)	56	70
Ingot casting	1.0	1.6	0.4	1.6	0.40	2.0
Total	-	-	-	37	58	95

(*) When anode carbon is regarded as a fuel.

2.2 Aluminum Industry Decarbonization

Due to the varying characteristics of the heavy industry, (i.e., almost every facility worldwide is different, producing a wide array of product qualities and variations), GHG intensity, trade exposure, cost sensitivity, and long-lived facilities, it is often referred to as the most challenging sector to decarbonize [30]. Despite the increasing pressure on the energy-intensive and trade-exposed industries to reduce energy consumption and GHG emissions but deep decarbonization of heavy industry remains a daunting task. Most studies suggest adopting technologies that can help industrial sectors transition to a net-zero emissions structure. Table 2 summarizes the best available technologies (BET) for decarbonization of the aluminum industry.

Table 2 Engineering and process improvement technologies that result in direct emissions reductions in the aluminum industry.

Recent Technology	Description	Value chain impact	Potential impact on direct emissions
Fluidized bed calciners	Fluidized bed calciner technology is technically feasible, many aluminum companies already use this technology.	Refining	CFB calciners are more energy-efficient than rotary calciners and can result in both energy and cost savings (as much as 30–35%) [23][81]
CCUS	Absorption-based CCUS technology could be used in primary aluminum production during the refining process to capture emissions from fossil fuel-based thermal energy generation and during the smelting process to capture CO_2 from carbon anode consumption (TRL 3–4) [84].	Refining, Smelting and Recycling	Up to 95% CO_2 gas is initially absorbed by a solvent and then desorbed [50]. Which could decrease 35% (0.5 Gt) of direct emissions using CCUS [19].
Inert anode	Inert anode is a technology still in development for an industrial scale (TRL of 4–5) [85]. It is an alternative to the carbon anodes that are used in electrolysis during aluminum smelting resulting in the formation of oxygen instead of carbon dioxide.	Smelting	Reduces around 10–15% of sectoral emissions – assuming the use of renewable energy [19].
Hydrogen	It is theoretically possible to use hydrogen as a fuel for industrial processes that require high temperature heat. However, currently, hydrogen consumption is very low (TRL 4–5) [86][95].	Refining	The use of hydrogen could be used to reduce up to 183 Mt of CO_2e annually of direct emissions [19].
Waste heat recovery	There is an opportunity to reduce energy consumption by implementing waste heat recovery systems. Some of the commercially available technologies include energy modulation technology by EnPot, shell heat exchangers from REEL International and heat pipes by Cronus [87][88][89].	Refining and Smelting	30%- 45% of the heat produced during the aluminum smelting process is lost as waste heat [82].

Concentrated solar thermal (CST)	CST heat might be integrated into the aluminum industry, for example focal point concentration. In 2019, Heliogen demonstrated at a concentrated solar facility that CSP technology can reach temperatures of more than 1,000ºC [90]. Another experimental study that is being conducted on solar-driven for the calcination of alumina with an improved product quality to avoid the discharge of combustion-derived CO_2 emissions at least during those periods when the solar resource is available (TRL 7) [38][95].	Refining and Recycling	Eight hours of solar operation has the potential to save one-third of alumina production GHG emissions (In 2010, amounted to 13.7 Mt CO_2-e/year) [83].

2.2.1 Decarbonization of the power supply

Electricity is the greatest opportunity for decarbonization, accounting for 66.7% of the industry's carbon emissions [30]. The transition to a more sustainable power supply can be fundamentally achieved through the use of both renewable energy and/or carbon capture utilization and storage (CCUS) technologies. From 2000 to 2019, Global reliance on renewable energy has increased 3.4-fold primarily due to the increasing affordability of renewable power [31]. The levelized cost of electricity (LCOE) of renewable technologies have become more competitive with fossil fuels as shown in Fig. 4 [32]. It is currently "below the range of LCOE for new coal-fired power plants" and "in the same range" as the operating cost of existing coal-fired power plants in India and China [33].

Most of the renewable energy sources used in aluminum smelting process in the world are hydro and geothermal power due to their ability to provide continuous 24/7 power. For example, Karmøy Technology Plant in Norway has generated a maximum of 4.0 kg CO_2-equivalents per kg of aluminum by using hydropower for electrolysis reaction which is one-fourth of the global average from mine to metal [35]. The increasing renewable power mix in the aluminum industry will require the integration of various renewable energy sources into their power generation. As the world's aluminum producers look to reduce their emissions, implementing energy storage solutions will be a challenge.

Energy storage solutions will be required to ensure that the power needs of the aluminum industry are met. Scalable CCUS can also reduce emissions at a similar rate as a transition to renewables. CCUS technologies are currently not widely available at the utility-scale, but they are expected to play a major role in helping the aluminum industry meets its emissions reduction goals. It is likely that, at least in the short to mid-term, a combination of transition to renewable sources and CCUS will be required to support the decarbonization of the aluminum industry [36].

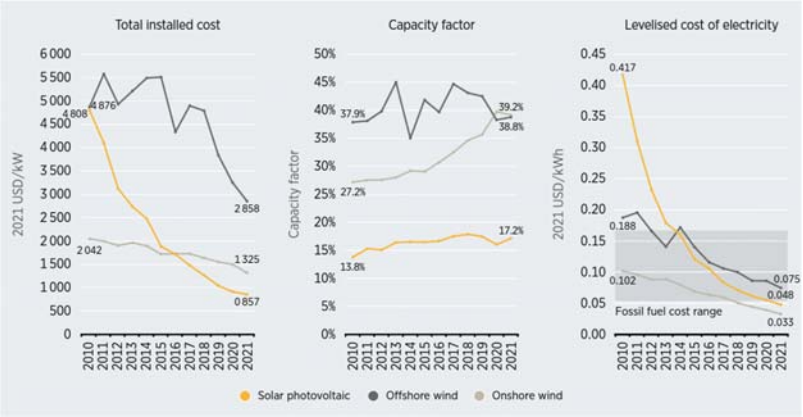


Fig. 4 Change in installed cost, capacity factor and LCOE of renewable sources (2010–2021) [32].

2.2.2 Decarbonization of process emissions

Although decarbonization of the direct emissions is relatively small compared to power consumption, they can be addressed in the production of primary aluminum specifically in alumina refining and electrolysis processes. Direct emissions from the production of primary aluminum are generated by the use of a carbon anode during the smelting process and by fuel combustion during the unit processes to produce heat and steam. In 2018, around 10% of sectoral emissions accounted for anode consumption and fuel combustion accounted for 15–20% of sectoral emissions [31]. The development of a non-carbon anode is a significant step towards decarbonization across the aluminum sector and transitioning to technologies that can provide heat and steam without the use of fossil fuels. The use of a non-carbon anode could reduce the direct emissions from the production of primary aluminum. Several aluminum producers including Rio Tinto, Alcoa, RUSAL, and Arctus Aluminum are currently working on developing anodes that can produce oxygen instead of carbon dioxide [37].

Aside from the development of a non-carbon anode, the production of alumina also requires large amounts of steam and heat to convert the raw materials into alumina during refining, currently primarily generated using fossil fuels. Alternative energy sources such as CSP, geothermal or hydrogen can be used to produce steam and heat. Davis, et al. [38] reported 5 kW novel solar transport reactor successfully demonstrated the experimental calcination of alumina utilizing concentrated solar thermal (CST). Yet no commercial demonstration of the calcination of gibbsite at flash calcination-relevant conditions has been documented. The industrial calcination of gibbsite shares parallels with the calcination of limestone which occurs at 1150 K and has been previously proven with the use of CST at those times when the solar

resource is accessible [39,40]. Although this technology is being explored for industrial use worldwide, it is still largely dependent on the geography of the region where it is located.

Low or zero-carbon hydrogen can help to decarbonize a range of sectors, including long-distance transportation, chemicals, and iron and steel, where it has been shown to be challenging to cut emissions. Fuel switching to green hydrogen (defined below) in the calcination process offers the most credible pathway. Rio Tinto has announced – with the support of Australia – a feasibility study for the use of hydrogen to generate the heat required for alumina refining at its Yarwun refinery. A lab-sized reactor was utilized to model the calcination process at Rio Tinto's Bundoora Technical Development Centre in Melbourne, Victoria. In order to comprehend the construction and operational needs of a potential refinery demonstration project, Rio Tinto Yarwun also carried out an initial engineering and design study [41]. Furthermore, hydrogen boilers have been explored widely lately. Hydrogen-ready boiler is the first burner for heat treatment furnaces operating at up to 100% hydrogen while maintaining NO_x emissions considerably below the toughest restrictions which was launched by Tenova [42]. Calcination furnaces and fuel nozzles have a significant impact on the level of NO_x emissions produced during alumina production. It is crucial to understand the various designs and operations of calcination furnaces and fuel nozzle design to control NO_x formation [67]. Since hydrogen combustion produces no carbon emission, it could significantly reduce calcination emissions depending on technical and retrofit considerations. In this regard, the study of decarbonizing the calcination process using renewable hydrogen is of great importance, particularly due to intensifying concern regarding global warming, and GHG emissions. The production of low or zero-carbon hydrogen using power-to-gas processes is introduced in Section 2.3.

2.2.3 Increased scrap recycling

Aluminum is an almost infinitely recyclable material; therefore, it is possible to recycle the remaining end-of-cycle scrap. In 2019, 34% of the aluminum produced came from new and old scrap (new scrap refers to scrap created during product manufacturing, while old scrap refers to end-of-life scrap) [43]. This could reduce the need for primary aluminum and carbon emissions associated with its production. In terms of energy consumption, the production of aluminum from scrap requires around 5% of the total energy needed to produce the primary aluminum. Consequently, waste that is kept for recycling can save the energy needed to produce primary aluminum by up to 95% [44]. Recycled aluminum accounts for around 33% of aluminum production, a relatively constant demand since 2000 [43].

As an example of decarbonization of aluminum-based products using scrap metal, in 2019, Novelis and Volvo partnered to develop and implement a closed-loop recycling system for the aluminum components of Volvo cars. This reduced Volvo's reliance on primary aluminum, decreasing the carbon intensity by 78% [45].

2.3 Power-to-Gas

Although hydrogen gas has neither a color nor an odor, it is now frequently identified by a color that links the gas's production process to its raw materials and emissions. Hydrogen comes in a variety of colors, which typically vary from grey to blue and even green. About 95% of the hydrogen gas generated today across the world comes from the steam methane reforming (SMR) process, which is mostly used to manufacture grey hydrogen from the reforming of fossil fuels like natural gas, liquefied petroleum gas (LPG), or naphtha [46]. Grey hydrogen has the lowest production costs, needs the least equipment, and has a low carbon footprint. However, as the SMR process produces CO_2 that is emitted into the atmosphere, its adoption is under pressure due to environmental concerns. Likewise, blue hydrogen is created using fossil fuels but has a lower carbon intensity due to the sequestration or reusing of the CO_2 that is released. A fraction of the CO_2 created during the process is captured and stored, and this can cut carbon emissions by up to 90%. The price of producing blue hydrogen is affected by feedstock, utilities, the additional costs associated with managing CO_2 (such as recovery, compression, storage, transport via pipelines, and sequestration), and the availability of carbon credits [47].

Green hydrogen is produced through water electrolysis using electricity generated from renewable resources, this process is also called Power-to-Gas and it has the lowest carbon footprint since clean energy is utilized to separate it from other substances like water molecules. The cost of the actual electrolysis process is the largest cost component, however, over the past ten years, the cost of producing renewable energy has decreased dramatically. Alkaline electrolyser is a mature, commercially available technology and is used in large-scale operations for its advantages. It has lower costs and longer durability; it also has lower flexibility with a minimum load requirement of 20 % to 40 % [46].

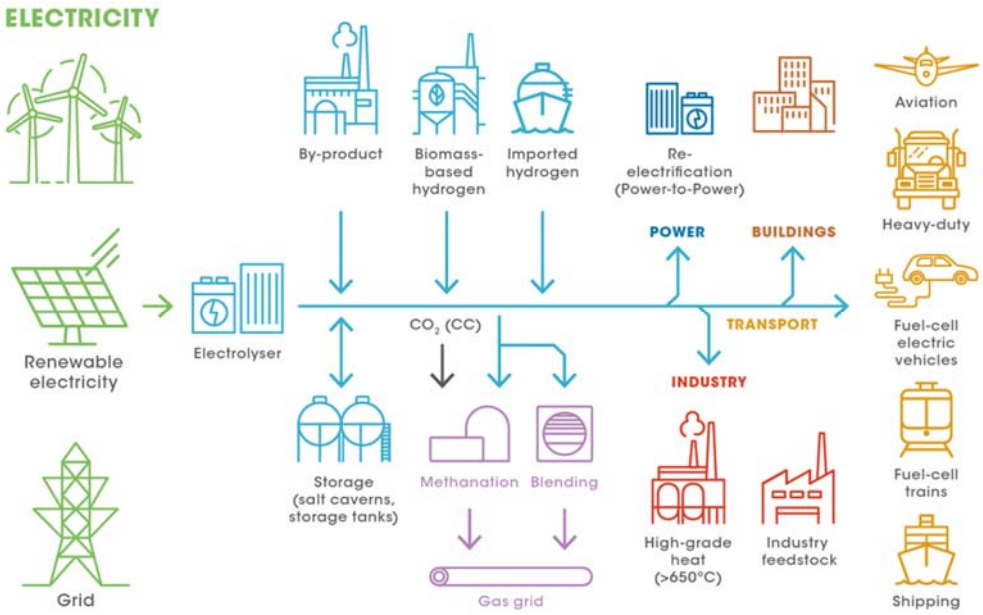


Fig. 5 PtH_2 concept, including hydrogen end-use applications [49].

2.4 Summary

Based on the literature review presented in Sections 2.1-2.3, the main research gap that has been identified regarding the decarbonization of the aluminum industry is the lack of focused studies on decreasing direct process emissions from aluminum making using green hydrogen.

3. Thesis Aim, Scope, Approach, Tasks and Expected Outcomes

The objectives, scope, overall approach, work packages, expected outcomes and deliverables of the proposed Thesis are presented in Sections 3.1-3.4.

3.1 Overall Aim

The overall aim of the Thesis research is to contribute to the decarbonization of primary aluminum manufacturing, by investigating the calcination process fueled by low-carbon hydrogen produced using power-to-gas to substitute for currently used fossil fuels, as well as using renewable electricity for alumina electrolysis.

3.2 Scope and Approach

The overall main of the Thesis research will be achieved through the design and modeling-based thermodynamic and environmental evaluation of low-carbon hydrogen production and conversion processes in aluminum making, focusing on substituting natural gas in alumina hydrate calcination, and electricity generation for alumina electrolysis by low-carbon energy sources. The thermodynamic and environmental characteristics of the proposed alternative processes are compared with those of conventional processes.

3.2.1 Alumina refining process and PtG process configurations

The calcination technologies considered focus on circulating fluidized beds, which is known to offer significant energy savings (~ 60%) compared to conventional rotary kilns [27]. For the PtH_2 process, low temperature electrolysis is selected for hydrogen production, which is generally considered the preferred technology for electrolysis projects due to its commercial maturity. The conventional process for alumina refining using NG and combustion of low-carbon hydrogen in CFB will be compared.

3.2.2 Energy sources for power-to-hydrogen and alumina electrolysis

The use of lower-carbon electricity for hydrogen production and aluminum smelting will be investigated.

3.2.3 Scheme thermodynamic, and environmental performance assessment

In the first step, a thermodynamic analysis is performed, and material and energy flows are calculated for key states of the conventional NG-based and power-to-hydrogen based

calcination system. Energy consumption for the calcination process per kg of alumina and the overall aluminum production process are evaluated, as well as CO_2 emissions per kg of alumina for the calcination process and for the whole aluminum production process per ton of Al.

3.2.4 Modeling approach

Simulation models of the conventional NG-based and power-to-hydrogen based calcination systems are constructed using programming software (e.g., MATLAB) and validated using published reference data.

3.3 Work Packages

The main work packages of the Thesis research are to evaluate emissions reductions for the green hydrogen-fueled fluidized bed system for the alumina calcination process for several locations with different renewable resources and grids. The main work modules are as follows:

1- Development and validation of a steady-state model of a NG-based calcination and aluminum smelting (electrolysis) processes.
2- Modification of the NG-based calcination process to substitute NG for hydrogen.
3- Energy and emissions analysis of the hydrogen- and NG-based calcination processes, and smelting process, for base-case design/operating parameters
4- Sensitivity analysis to evaluate the energy, and emissions of the hydrogen-based calcination and smelting processes as a function of key design/operating parameters.

3.4 Expected Outcomes and Deliverables

The outcomes and deliverables of the Thesis are as follows:

1. Proposed power-to-hydrogen based calcination process scheme.
2. Validated model for NG- and hydrogen-based calcination, and aluminum smelting processes.
3. Quantification of energy consumption, and emissions for the hydrogen-based calcination process in comparison with conventional NG-based calcination.

4. Power-to-Hydrogen Alumina Hydrate Calcination Scheme

Fig. 6 and 7 illustrate the proposed low-carbon alumina hydrate and the conventional NG-based calcination and alumina electrolysis processes configurations, respectively. The latter includes a low-temperature water electrolysis plant, and calciner and alumina electrolyser sub-systems.

As a base case, the integrated PtH_2 aluminum production plant is powered by grid electricity. On-site solar PV will be subsequently considered. Low-temperature water electrolysis (LTE) is chosen for the production of low-carbon hydrogen due to the technology's maturity and economic viability [50]. According to reaction (1), liquid water (H_2O) is electrolyzed at atmospheric pressure in the LTE to produce H_2 and oxygen (O_2). In the calcination, boehmite ($Al_2O_3 \cdot H_2O$) is dehydrated to alumina (Al_2O_3) according to reaction (2) [67]. The dehydration path of boehmite is subsequently transformed into a mixture of crystalline transition phase alumina consisting mostly of α- and γ-alumina. The formation of the alpha phase from the gamma phase is exothermic and is controlled only by reaction kinetics. Industrial smelter-grade alumina (SGA) contains about 2-10% of the alpha phase, exceeding this range may affect the integrity of the smelting pot crust making it weaker and more difficult to keep the pot sealed. Generally alpha content of less than 6% is preferred by most smelting clients [67]. In this model, the SGA formed is assumed to be 100% γ-alumina. The heat for calcination is provided by the combustion of hydrogen fuel in the calciner furnace (reaction (3)). For the conventional process, methane is used for the heat input (see Fig. 7). In reaction (5), the alumina reacts with carbon anode to produce pure aluminum and CO_2.

$$H_2O_{(l)} \rightarrow H_{2(g)} + \frac{1}{2}O_{2(g)} \qquad \Delta H^0_{298\,K} = +285.83\,\frac{kJ}{mol\,H_2O} \quad (1)$$

$$2Al_2O_3 \cdot H_2O_{(cr)} + \text{Heat} \rightarrow H_2O_{(g)} + Al_2O_{3(cr)} \qquad \Delta H^0_{298\,K} = +109.23\,\frac{kJ}{mol\,Al_2O_3}\,[67] \quad (2)$$

$$H_{2(g)} + \frac{1}{2}\left(O_{2(g)} + 3.76\,N_{2(g)}\right) \rightarrow H_2O_{(g)} + 1.88\,N_{2(g)} \qquad \Delta H^0_{298\,K} = -241\,\frac{kJ}{mol\,H_2} \quad (3)$$

$$CH_{4(g)} + 2\left(O_{2(g)} + 3.76\,N_{2(g)}\right) \rightarrow CO_{2(g)} + 2H_2O_{(g)} + 7.52N_{2(g)} \qquad \Delta H^0_{298\,K} = -802.30\,\frac{kJ}{mol\,CH_4} \quad (4)$$

$$2Al_2O_{3(c)} + 3C_{(s)} + \text{Electricity} \rightarrow 4\,Al_{(l)} + 3CO_{2(g)} \qquad \Delta H^0_{1000\,K} = +542.6\,\frac{kJ}{mol\,Al}\,[76] \quad (5)$$

The calciner operates at a typical temperature of 1223.15 K (950 ºC) [22][23][67]. The alumina wet hydrate is dried through preheating stages from ambient conditions at 298.15 K (25 ºC) (state 1) [67] to the dry hydrate temperature calculated by the model at state 3 by exchanging

the heat from top gases exiting the calciner at typical operating temperature of the calciner (state 19) thereby condensing the top gas water content formed in the calcination and combustion reactions which could be recycled to the electrolysis plant. The top gases exit the preheating stages at state 21 at prescribed typical temperature 433.15 K (160 ºC) [22][23][67][69]. The alumina produced through calcination enters the cooling cyclones (state 4) for pre-heating the combustion inlet air (secondary air) from 298.15 K (25 ºC) (state 16) to the temperature at state 18 which is calculated by the model. Secondary air is fed relative to the stoichiometry of reaction (4), and to ensure a complete combustion, the fluidization air (primary air) in stream 15 is assumed to be used which is significantly exceeds the requirement with no further excess air required. The cooled alumina exits the final cooling stage (i.e., fluid bed cooler) at a prescribed temperature 353.15 K (80 ºC) (state 7) [67] and is continuously loaded into the aluminum electrolyser for processing into liquid aluminum (state 8). In this model the streams between the 2 stages of preheating and cooling are not considered and preserved as a block as shown in Fig 6, and 7. The alumina electrolyser takes as energy input electricity and carbon as feedstock to form liquid aluminum at 1223.15 K (950 ºC) (state 8) [21][51]. The aluminum electrolyser off-gases are assumed to exit at the same temperature. The addition of carbon (45 kg/kg Al) serves several purposes, including reducing the Al_2O_3 exiting the aluminum smelting process into pure aluminum (reaction (5)). For operation on low-cost electricity or renewable electricity, electrolytic H_2 produced in excess of the calciner H_2 demand can be compressed to what pressure and stored in the high-pressure H_2 storage sub-system for subsequent use in the calcination process in high electricity price periods or low renewable electricity availability.

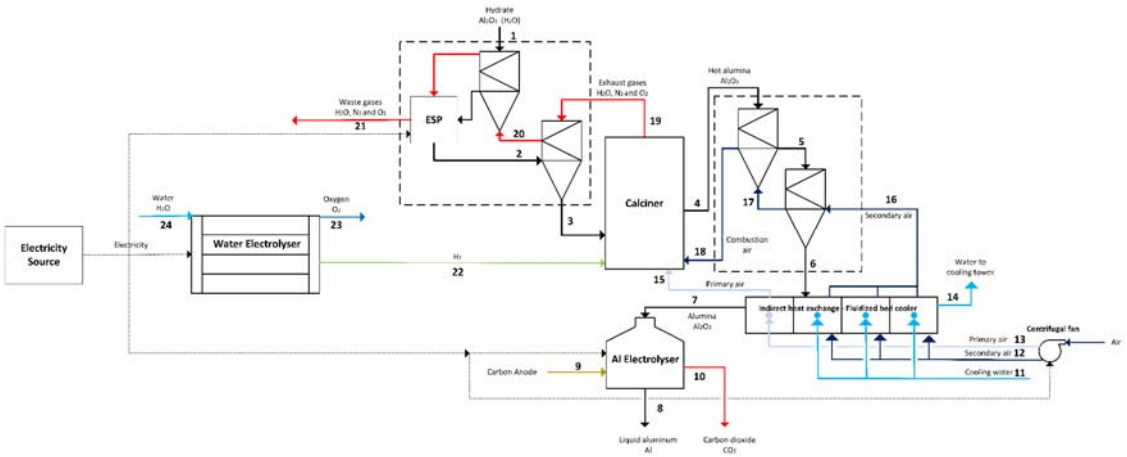


Fig. 6 Schematic of the Hydrogen calciner furnace coupled with an aluminum smelting process (electrolysis). LTE electrolyser is considered for hydrogen production.

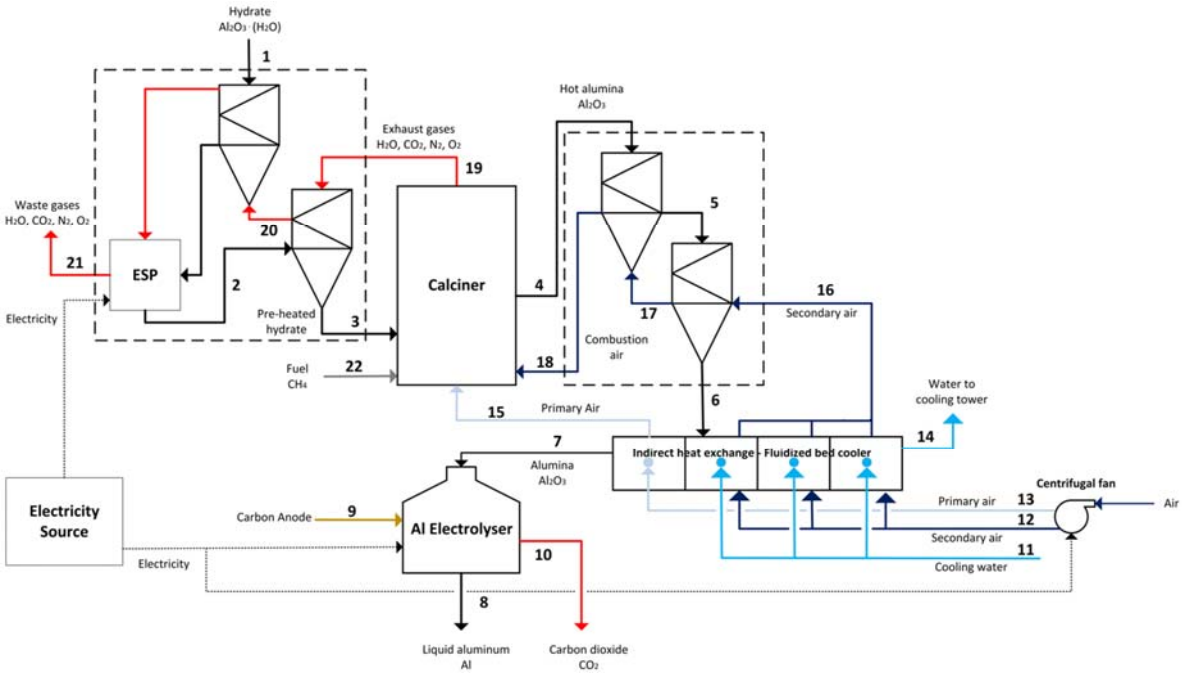


Fig. 7 Schematic of the conventional calciner furnace fueled by natural gas coupled with an aluminum smelting process (aluminum electrolysis).

5. Modeling and Analysis Methodology

The energy consumption, carbon intensity, and operational characteristics of H_2-based calcination and aluminum production processes configuration in Fig. 6 are investigated and compared with the conventional NG-based calcination process (Fig. 7). The model incorporates a steady-state material and energy process sub-model. The main modeling assumptions, input parameters, and system performance metrics are documented in this section. The main modeling assumptions for the process configuration in Fig. 6 and 7 are as follows:

- Steady state operation.
- The type of hydrate entering the calciner is boehmite ($Al_2O_3 \cdot H_2O$), which can result in 60% fuel reduction during the calcination stage compared to other types of bauxite [54][76].
- The total percentage of impurities (i.e., Na_2O, CaO, Fe_2O_3, and SiO_2) for each in boehmite, alumina and aluminum are 1.2% [55], 0.8% [56][67] and 0.01% [57].
- Rich combustion is assumed in the calciner furnace provided through the mass flow air required for the fluidization which significantly exceeds the requirement with no further excess air required.
- The natural gas fuel is assumed to be 100% methane (CH_4).
- Material flows through the system units are based on stoichiometry; calcination and alumina electrolysis chemical reactions proceed to completion in a single pass.
- Gases (H_2O, N_2 and O_2) exiting the pre-heating stage is at temperatures above water dew point [22].
- Gas–solid heat capacity flow ratio ($\dot{m}C_p$), ϕ = 1 [67].
- Ambient temperature (25°C) was used as the reference temperature; therefore, sensible heat of normal temperature materials and air entering the system, such as inlet materials (alumina hydrate, carbon anode, and water cooling) and air, can be ignored.
- The present calciner is assumed to be CFB type and adiabatic, i.e., no heat loss to the surroundings from the calciner. (Actual calciners have energy efficiencies of 92-95%, with 5-8% as heat loss [23][69][100]).
- LTE electrolyser system is used for the production of hydrogen with a HHV efficiency of 0.8 [53].
- Grid electricity production emissions (used for H_2 production via electrolysis, and alumina smelting) is assumed as 10 (gCO_{2eq} per kWh) for the base case.

- The energy consumption and emissions of hydrogen compression and storage are not considered for steady-state operation.
- Increase in internal vapour pressure in the reactor is neglected.
- Enthalpy of vaporization of water taken at ambient temperature (i.e., 25°C).

5.1 Analyses

5.1.1 CFB calciner

CFB have experienced several advancements and continuous development since they were initially introduced more than 40 years ago. Numerous research efforts were put into these technologies due to the possible benefits in fuel energy savings, higher production volumes, decreased maintenance whilst retaining equivalent product quality, etc. As a consequence, several versions of the fluidized bed technology emerged. Figure 8 demonstrates how, from the initial inception of the Bayer calcination process to the present, this particular unit operation has seen a 50% drop in specific energy usage despite significant changes in technical approach. It should be noted that the predicted energy consumption does account for the hydrate's surface moisture but excludes heat losses and assumes all energy is used for the calcination operations [90][100].

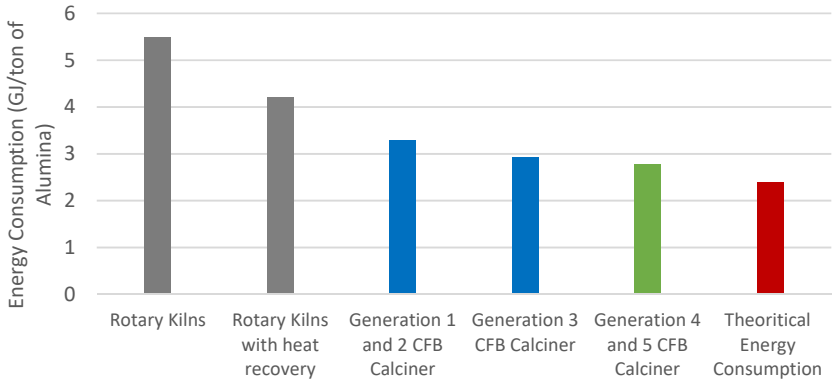


Fig. 8 Progressive drop in specific energy consumption versus calciner technology [100].

In this model, the generation 4 CFB calciner flowsheet was selected (see Fig 9). The CFB calciner has two-stages front end for preheating the alumina hydrate before entering the calciner and it is equipped with direct heat recovery stages followed by a large fluid bed cooler.

5.1.1.1 Preheating stages

The hydrate is preheated using the CFB furnace's top-gases in two stages in the present flowsheet. The hydrate's free moisture, which typically ranges from 6 to 8% moisture

[23][67][76], is evaporated, and dried during the first preheating stage. Afterward, the dried hydrate is separated from the gas in an electrostatic precipitator and sent to the second preheating stage, where it is mixed with the furnace's 950°C hot top-gases. Here, a substantial phase of the reaction is already underway with the release of around two-thirds of the hydrate water.

The solids are once again separated from the gas and brought to the CFB furnace. The pre-calcined material is finally calcined to the desired alumina grade in the CFB furnace under the high solid's density, homogenous mixing, and temperature field. The optimum product quality, with extremely little alpha alumina (~0%) and no residual boehmite as well as minimum particle breakage, is made possible by the effective mixing and high solids density combined with a suitable residence period of several minutes.

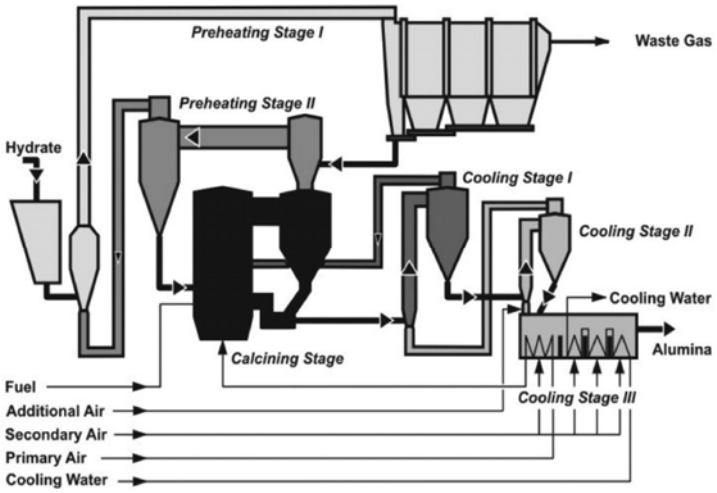


Fig. 9 Outotec-circulating fluid bed calciner generation 4 flowsheet [23].

Using equation 6, the inlet hydrate temperature to the preheating stage $T_{1,h}$ = 25°C, the temperature of hot gases exciting the calciner $T_{19,g}$ = 950 °C, the temperature of waste gases exiting preheating zone and electrostatic precipitator (ESP) $T_{21,g}$ = 160 °C [22][23][67], theoretical thermal efficiency of direct heat transfer (DHT) for the preheating $\eta_{p,h}(\%)$ can be calculated and it is found to be 85.4%.

$$\eta_{p,h} = \frac{T_{19,g} - T_{21,g}}{T_{19,g} - T_{1,h}} \tag{6}$$

The dry hydrate temperature after preheating is obtained then assuming the heat capacity flow ratio between gases and solids (φ) to be 1.

$$T_{3,d,h} = T_{1,h} + \frac{\eta_{p,h}}{\varphi} (T_{19,g} - T_{1,h}) \tag{7}$$

5.1.1.2 Cooling stages

After discharge from the CFB calcining stage, the hot alumina is cooled in three stages: two direct gas solids contact cooling stages, and one indirect cooling stage, the fluid bed cooler. In the first two phases of cooling, secondary air is mixed with hot alumina, which causes the air to heat up while the alumina cools. Raahauge et al. has reported the effect of the number of direct heat transfer (DHT) for cooling stages N on the theoretical thermal efficiency [67]. The theoretical thermal efficiency for cooling, η_c (%), increases with number of DHT stages N, and the theoretical heat loss from alumina to the fluid-bed cooling water (Q_{FBC}) decreases significantly. Two direct heat recovery stages were applied for the base case model with 67% efficiency [67]. The theoretical thermal efficiency equation is given by $\eta_c = \frac{T_{4,ala} - T_{6,ala}}{T_{4,ala} - T_{16,s,a}}$, where $T_{6,ala}$ is the theoretical alumina inlet temperature to the fluid bed cooler, $T_{4,ala}$ is the hot alumina temperature after calcination process and $T_{16,s,a}$ is the inlet secondary air temperature assumed to be 25 °C. Therefore, the temperature of alumina discharged from DHT stages ($T_{6,ala}$) and the preheated secondary air temperature ($T_{18,s,a}$) are calculated as follow [67].

$$T_{6,ala} = T_{4,ala} - \eta_c (T_{4,ala} - T_{16,s,a}) \quad (8)$$

$$T_{18,s,a} = T_{16,s,a} + \frac{\eta_c}{\varphi} (T_{4,ala} - T_{16,s,a}) \quad (9)$$

The preheated secondary air from each stage is directed toward the downstream inlet points of lower CFB furnace where it is used as hot combustion air before being separated from it by a gas cyclone and then the combustion is completed by the primary air stream under an excess of 5 to 10% above stoichiometric at the upper section of the furnace [101].

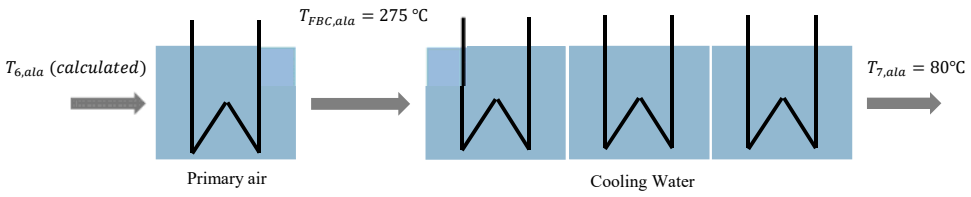


Fig. 10 Conceptual fluid bed cooler with the hot-end section (primary air heating), and cold-end section (final alumina product cooling). Also, the expected solids temperatures between the different stages are indicated, re-drawn based on [22].

Lastly, in the fluid bed cooler, all the alumina's surplus heat that was difficult to recover during the DHT process is removed, enabling discharge at temperatures that are safe for handling. The fluid bed cooler consists of two sections, “hot-end” section for indirectly preheating primary air required for fluidization of the alumina in the CFB reactor and the final cooling of the

alumina takes place indirectly with cooling water in the "cold-end" section to safe handling temperatures ~80°C [22]. The cooling water is heated from 25°C to 40°C.

The air mass flow to the calciner includes both the primary air for fluidization and the secondary air based on the stoichiometry of the natural gas or hydrogen combustion reaction. The primary air mass flow requirement for fluidization can be calculated for on the flow regime, particle fluidization velocity, v, Reynolds number, Re, and Archimedes number, Ar [97]. These quantities depend on the particle diameter, particle and fluid (air) densities, and fluid dynamic viscosity. The alumina and air properties are taken at operating calcination conditions (950 °C).

Particle size affects the calcination process and, consequently, the heating rates, which are both extremely varied. As of the particle breakdown that occurs during calcination, the particle size distribution of the hydrate changes when it is calcined in industrial calciner units at various temperature profiles and gas velocities. The number of fines (< 45 μm) and super fines (< 20 μm) produced during calcination are (<10 wt%) and (1-2 wt%) as reported in Raahauge the rest is >250 μm. To ensure a conservative approach, a large particle size of 250 μm is used to calculate minimum fluidization velocity [67][90][98]. By assuming spherical particles and settling in a laminar flow regime (Stokes law) [97] where relatively small particles are moving in a fluid (air) and the Reynolds number is low, Re <<1, the minimum fluidization velocity (v_{min}) can be calculated using the following equation from [97].

$$v_{min} = \frac{g d_p^2 (\rho_p - \rho_f)}{18 \mu_f} \tag{10}$$

$$Re = \frac{d_p \rho_f v_{min}}{\mu_f} \tag{11}$$

Where g is the gravitational acceleration (9.81 m/s^2), d_p is the particle diameter (250 μm assumed), ρ_p is the hydrate particle density (3000 kg/m^3), ρ_f is the fluid (air) density (0.289 kg/m^3), μ_f is the fluid (air) dynamic viscosity (4.7125×10^{-5} kg/m·s) as documented in Table 3). The particle size For Re >>1, the settling is turbulent, and the fluidization velocity can be calculated based on Archimedes and Reynolds numbers as follows [97]:

$$Ar = \frac{\rho_f g d_p^3 (\rho_p - \rho_f)}{\mu_f^2} \tag{12}$$

$$Re = 0.1334 Ar^{0.7016} \tag{13}$$

$$v_{min} = \frac{Re\mu_f}{\rho_f d_p} \tag{14}$$

Where Ar is the Archimedes number. The calculated Reynolds number indicates turbulent flow regime, and a minimum velocity of 1.5356 m/s is found.

The mass flow rate of primary air ($\dot{m}_{pri,a}$) is highly dependent on the cross-sectional area of the CFB calciner (A). According to [96], the entire area of the CFB calcining plant measures approximately 23×18 m² for a calciner that has a production capacity of 3500 tons of alumina per day. This is almost equivalent to a model production capacity of approximately 3990 tons of alumina per day, based on a 95% capacity utilization rate. However, since there is a shortage of the reactor scale data in the literature, the developed model assumes that the reactor is made up of well-mixed volumes in series, even though industrial calciners may have complex flow patterns [99]. It is assumed in this work that the calciner furnace cross sectional area occupies approximately 20% of the total surface area of a vertical CFB system layout based on visual observation [110], which is approximately 83 m² [96]. Therefore, the primary flow rate of air mass can be calculated using equation (15).

$$\dot{m}_{pri,a} = \rho_f v A \tag{15}$$

$$= (0.289)(1.5356\ )(83) = 36.7464\ \frac{kg\ of\ air}{s} = 0.0367 \frac{ton\ of\ air}{s}$$

$$M_{15,p,a} = 0.0367 \frac{t\ air}{s} \times \frac{3600 s}{hr} \times \frac{hr}{175\ t\ ala} = 0.7559 \frac{t\ air}{t\ ala} = 1.4398 \frac{t\ air}{t\ Al}$$

The theoretical heat loss from alumina to the air ($Q_{FBC,h,e}$) and the fluid-bed cooling water ($Q_{FBC,c,e}$) are calculated using the enthalpy change of alumina cooled step by step as explained in Fig. 9.

$$Q_{FBC,h,e} = M_{7,ala}(\Delta h_{6,ala} - \Delta h_{FBC,ala}) \tag{16}$$

$$Q_{FBC,c,e} = M_{7,ala}(\Delta h_{CFB,ala} - \Delta h_{7,ala}) \tag{17}$$

$$Q_{FBC} = Q_{FBC,h,e} + Q_{FBC,h,e} \tag{18}$$

Several large centrifugal blowers are used to supply all the air needed for combustion and fluidization, passing through the fluid-bed cooler with specific energy of 19 kWh/t alumina [67]. To ensure a low formation of NO_x at the elevated reactor temperature, part of primary air from the indirect cooling stage is used which results in a two (2) stage combustion process. The temperature of preheated primary air is found using the $Q_{FBC,h,e}$ equation.

$$T_{15,p,a} = \frac{Q_{FBC,h,e}}{M_{15,p,a} C_{p,air}} + T_{13,p,a} \quad (19)$$

To find the amount of cooling water in kg/t Al, the theoretical heat loss from alumina to the fluid-bed cooling water ($Q_{FBC,c,e}$) is found. Where $T_{11,w}$ and $T_{14,w}$ are the inlet and outlet temperature of the water cooling respectively. Approximately resulted 6.3591 ton of cooling water/tAl.

$$M_{11,w} = \frac{Q_{FBC,c,e}}{C_{p,w}(T_{14,w} - T_{11,w})} \quad (20)$$

Finally, the effectiveness of the fluid bed-cooler (ϵ) is estimated for each section (hot and cold-end) by equating the heat lost by alumina to the heat gained by air/water, using their respective specific heat capacities calculated at average temperatures (eq. 21 & eq.22). The primary air part is indirectly preheated with an effectiveness of 0.2174, and alumina is cooled with water at an effectiveness of 0.78.

$$\epsilon_{FBC,h,e} = \frac{(Mc_p)_{ala}(T_{ala,in} - T_{ala,out})}{(Mc_p)_{min}(T_{max} - T_{min})} = \frac{(Mc_p)_{air}(T_{air,out} - T_{air,in})}{(Mc_p)_{min}(T_{max} - T_{min})} \quad (21)$$

$$\epsilon_{FBC,c,e} = \frac{(Mc_p)_{ala}(T_{ala,in} - T_{ala,out})}{(Mc_p)_{min}(T_{max} - T_{min})} = \frac{(Mc_p)_{w}(T_{w,out} - T_{w,in})}{(Mc_p)_{min}(T_{max} - T_{min})} \quad (22)$$

5.2 Thermodynamic Process Model

The thermodynamic process model is based on steady-state mass and energy conservation applied to each system component considered as a control volume, for which the generic relations are given in equation 23 and 24:

Overall mass balance:

$$\sum m_{in} = \sum m_{out} \quad (23)$$

Overall energy balance:

$$\sum m_{in} h_{in} - \sum m_{out}\, h_{out} + Q - W = 0 \quad (24)$$

where h refers to specific enthalpy in kJ/kg. Enthalpies (in kJ/mol) of water/steam, carbon dioxide, carbon, hydrogen, alumina hydrate, alumina and aluminum are evaluated using the Shomate equation (equation 25) with coefficients (A, B,.., H) obtained from NIST for water/steam, [70], hydrogen [71], carbon dioxide [72], alumina hydrate [73], alumina [74] and aluminum [75]:

$$H^0 - H^0_{298K} = A\,t + \frac{B\,t^2}{2} + \frac{C\,t^3}{3} + \frac{D\,t^4}{4} - \frac{E}{t} + F - H \quad (25)$$

where H refers to enthalpy in kJ/mol, and t is the non-dimensional temperature given by:

$$t = temperature\ (K) / 1000$$

The PtH_2 calcination- aluminum electrolysis and conventional process input modeling parameters are documented in Tables 3. Material, temperature, and energy for each stream are evaluated based on the stoichiometry and enthalpies of reactions (1–5), in Tables 1a and 2a.

Table 3. Input modeling parameters for calcination-alumina electrolysis.

Parameter	Range	Selected value	Reference
Liquid aluminum (ton/t Al)	1	1	
Alumina hydrate purity (wt %)	98.5-99	98.8	[55]
Alumina purity (wt %)	98.5-99.7	99.2	[56][67]
Moisture content in alumina hydrate (wt %)c	6-8	6	[23][67][76]
Outlet temperature of waste gases leaving the electrostatic precipitator (℃)	150-170	160	[22][23][67][69]
Calciner alumina hydrate pre-heating stages efficiency (%) (equation 6)	Calculated	-	-
Inlet temperature of hydrate in preheating stages (℃)	25	25	-
CFB calciner operating temperature (℃)	950-1100	950	[21][23][51][67][69][100]
Calcination reaction enthalpy (kJ/kg Al_2O_3) (reaction 2)	1071.33 1127.9 (115 kJ/mol Al_2O_3)	1071.33	[67] [76]
Inlet temperature of CH_4 to the calciner (℃)	25	25	-
CH_4 lower heating value (LHV) (MJ/kg CH_4)	50	50	[77]
Specific thermal energy consumption of conventional calciner (GJ/tAl)	Calculated	-	-
CH_4 consumption in CFB calciner (t/tAl)	Calculated	-	-
Lumped efficiency of 2 stages CFB alumina cooling stage (%) (equation 8)	67-80	67	[67]
Power consumption for air blowers and ESP in calcination process (kWh/ tAl_2O_3)	18-20	19	[100]
Fluid bed cooler effectiveness (%) (equation 21 & 22)	Calculated	-	-
Alumina discharge temperature from fluid bed cooler (℃)	80	80	[22][67][101]
Inlet temperature of primary and secondary air in FBC (℃)	25	25	-
Inlet temperature of FBC cooling water (℃)	25	25	-
Smelter anode carbon mass consumption efficiency (%)	70-80	75	[102]
Smelter aluminum electrolysis current efficiency (%)	95-98.5	96	[67][4][12]
Smelter aluminum electrolysis operating temperature (℃)	950	950	[4][10][11][17]
Alumina electrolysis reaction enthalpy (MJ/kg Al) (reaction 5)	20.384 20.112	20.112	[93] [76]
Outlet temperature of exhaust gas from aluminum electrolyser (℃)	950-960	950	[11][29][67][76]
Smelter aluminum electrolysis SEC (MWh_e/ tAl)	Calculated	-	-
Lower heating value of hydrogen (LHV) (MJ/kg H_2)	120	120	[77]
Specific thermal energy consumption of H_2 fueled calciner (GJ/tAl)	Calculated	-	-
H_2 consumption in CFB calciner (t/tAl)	Calculated	-	-
Water electrolysis efficiency (%)	80	80	[53]
Water electrolyser SEC (GJ/tAl)	Calculated	-	-
CFB furnace particle diameter (μm)	50-1000	250	[67][90][98]
Air dynamic viscosity at calciner operating temperature 950℃ (kg/m·s)	4.7125×10^{-5}	4.7125×10^{-5}	[103]
Air density at calciner operating temperature 950℃ (kg/m^3)	0.289	0.289	[103]
Alumina hydrate density (kg/m^3)	3000	3000	[104]
Enthalpy of vaporization of water at 25 °C and 1 bar absolute pressure (MJ/tH_2O)	2441.7	2441.7	[105]

The proposed model of the PtH_2 and conventional calcination- and alumina electrolysis processes in Fig. 6 and Fig. 7 were validated based on several output variables. As a first step,

the model predictions of each stream specific enthalpy with the corresponding values from thermodynamic tables [63][64][65] were compared. Tables 4 and 5 present the predictions of substances for NG-based, PtH_2-based calcination and aluminum smelting processes. The average deviation between modeling predictions and reference data for the NG-calciner and aluminum smelting processes is 0.36%, indicating a good match. The average deviation between modeling predictions and reference data for the PtH_2-calciner and aluminum smelting processes is slightly higher (0.64%), because the maximum deviation for the PtH_2-based process occurred at state 22.

Table 4. Prediction discrepancy between the present model and thermodynamic property tables for NG-based calcination and aluminum smelting processes.

Stream	Substance	Temperature (K)	Specific enthalpy, *h* (MJ/kg)		Prediction discrepancy
			Predicted using Shomate equation	Thermodynamic Tables [63,64,65]	
1	Alumina hydrate ($Al_2O_3 \cdot H_2O$)	298.15	0	0	0
3	Alumina hydrate ($Al_2O_3 \cdot H_2O$) (gas state)	1088.2	0.8586	0.85656	0.00204 (0.2382%)
4	Alumina (Al_2O_3)	1223.15	1.0860	1.06646	0.01954 (1.8322%)
6	Alumina (Al_2O_3)	603.4	0.3121	0.30608	0.00602 (1.9668%)
7	Alumina (Al_2O_3)	353.15	0.0474	0.04603	0.00137 (2.9763%)
8	Aluminum (Al)	1223.15	1.0129	1.01287	0.00003 (0.0029%)
9	Carbon Anode (C)	298.15	0	0	0
10	Carbon dioxide (CO_2)	1223.15	1.0403	1.04039	0.00009 (0.0086%)
11	Cooling water (H_2O)	298.15	0	0	0
12	Secondary air	298.15	0	0	0
13	Primary air	298.15	0	0	0
14	Water (H_2O)	548.4	0.4797	0.48150	0.00183 (0.3800%)
15	Primary air	338.5825	0.0410	0.04102	0.00002 (0.0488%)
16	Secondary air	298.15	0	0	0
18	Preheated secondary air	917.9	0.6598	0.66026	0.00046 (0.0697%)
19	Water vapor (H_2O)	1223.15	1.9718	1.97089	0.00091 (0.0462%)
	Carbon dioxide (CO_2)		1.0403	1.04039	0.00009 (0.0086%)
	Nitrogen (N_2)		1.0301	1.02981	0.00029 (0.0282%)
	Oxygen (O_2)		0.9558	0.95595	0.00015 (0.0157%)
21	Water vapor (H_2O)	433.15	0. 5704	0.57061	0.0021 (0.0368%)
	Carbon dioxide (CO_2)		0.1225	0.12158	0.00092 (0.7567%)
	Nitrogen (N_2)		0.1406	0.13872	0.00188 (1.3552%)
	Oxygen (O_2)		0.1259	0.12598	0.0008 (0.6350%)
22	Methane (CH_4)	298.15	0	0	0

Table 5. Prediction discrepancy between the present model and thermodynamic property tables for PtH_2-based calcination and aluminum smelting processes.

Stream	Substance	Temperature (K)	Specific enthalpy (MJ/kg)		Prediction discrepancy
			Predicted	Thermodynamic tables	
1	Alumina hydrate ($Al_2O_3 \cdot H_2O$)	298.15	0	0	0
3	Alumina hydrate ($Al_2O_3 \cdot H_2O$) (gas state)	1088.2	0.8586	0.85656	0.00204 (0.2382%)
4	Alumina (Al_2O_3)	1223.15	1.0860	1.06646	0.01954 (1.8322%)
6	Alumina (Al_2O_3)	603.4	0.3121	0.30608	0.00602 (1.9668%)
7	Alumina (Al_2O_3)	353.15	0.0474	0.04603	0.00137 (2.9763%)
8	Aluminum (Al)	1223.15	1.0129	1.01287	0.00003 (0.0029%)
9	Carbon Anode (C)	298.15	0	0	0
10	Carbon dioxide (CO_2)	1223.15	1.0403	1.04039	0.00009 (0.0086%)
11	Cooling water (H_2O)	298.15	0	0	0
12	Secondary air	298.15	0	0	0
13	Primary air	298.15	0	0	0
14	Water (H_2O)	548.4	0.4797	0.48150	0.00183 (0.3800%)
15	Primary air	338.5825	0.0410	0.04102	0.00002 (0.0488%)
16	Secondary air	298.15	0	0	0
18	Preheated secondary air	917.9	0.6598	0.66026	0.00046 (0.0697%)
19	Water vapor (H_2O)	1223.15	1.9718	1.97089	0.00091 (0.0462%)
	Nitrogen (N_2)		1.0301	1.02981	0.00029 (0.0282%)
	Oxygen (O_2)		0.9558	0.95595	0.00015 (0.0157%)
21	Water vapor (H_2O)	433.15	0. 5704	0.57061	0.00021 (0.0368%)
	Nitrogen (N_2)		0.1406	0.13872	0.00188 (1.3552%)
	Oxygen (O_2)		0.1259	0.12598	0.0001 (0.0794%)
22	Hydrogen (H_2)	343.15	0.6466	0.60184	0.04476 (7.4372%)
23	Hydrogen (H_2)	343.15	0.6466	0.60184	0.0001 (0.0241%)
26	Oxygen (O_2)	343.15	0.0415	0.04149	0
27	Water (H_2O)	298.15	0	0	0

5.2.1 Calciner specific energy consumption calculation

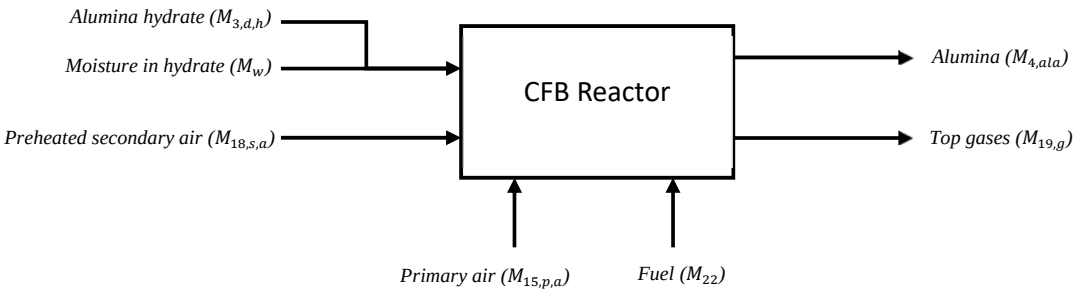


Fig. 11 Calcination of alumina hydrate process.

The mass of fuel (NG or H_2) required per ton of alumina produced or corresponding amount of aluminum required for the calcination process is calculated using the steady-state energy (heat) balance for the calciner in equation 26 expressed per ton of aluminum [67].

$$M_{3,d,h}\Delta h_{3,d,h} + M_w\Delta h_{3,w} + M_{18,s,a}\Delta h_{18,s,a} + M_{15,p,a}\Delta h_{15,p,a} + SEC_{cal} = M_{19,g}\Delta h_{19,g} + M_{4,ala}\Delta h_{4,ala} + M_w H_{vap} + \Delta H_{cal} \quad (26)$$

The mass flow rate of fuel M_f, is included in the following term of equation (26):

$$SEC_{cal} = M_f\left(\Delta h_f + LHV_f\right) \quad (27)$$

The mass flow rate of secondary (combustion) air $M_{18,s,a}$ and the mass flow rate of calciner exhaust gases $M_{19,g}$ are expressed in terms of the mass flow rate of fuel M_f, in order to solve for M_f using equation (26). The calculated value of M_f is then used to calculate the calciner SEC using equation (27). The specific enthalpy difference of the fuel at the calciner inlet Δh_f ($h - h^0_{298K}$ in kJ/kg) is not significant compared to the fuel chemical energy LHV_f. In this instance, NG enters the calciner at ambient temperature and consequently $\Delta h_f = 0$, while H_2 enters the calciner at the LTE exit temperature (70°C).

In equation (26), $M_{3,d,h}$ and $\Delta h_{3,d,h}$represent the mass and specific enthalpy difference ($h - h^0_{298K}$ in kJ/kg) as per the Shomate equation of the dry hydrate entering the calciner after the hydrate preheating stages, M_w and $\Delta h_{3,w}$ are the mass and specific enthalpy difference of the water content in the hydrate, $M_{18,s,a}$ and $\Delta h_{18,s,a}$ are the mass and specific enthalpy difference of the secondary air exciting cooling stages, $M_{15,p,a}$ and $\Delta h_{15,p,a}$ are the mass and specific enthalpy difference of primary air entering the calciner, $M_{19,g}$ and $\Delta h_{19,g}$ is the mass and specific enthalpy difference of exhaust gases (CO_2, H_2O, air and N_2) formed by both the calcination and combustion reactions (2, 3 & 4 respectively), $M_{4,ala}$ and $\Delta h_{4,ala}$ is the mass and specific enthalpy difference of hot alumina produced, H_{vap} is the vaporization enthalpy of the water content in the hydrate, ΔH_{cal} is the calcination reaction enthalpy.

To find the specific thermal consumption, the equation can be formulated as equation below.

$$SEC_{cal} = (M_{19,g}\Delta h_{19,g} + M_{4,ala}\Delta h_{4,ala} + M_w H_{vap} + \Delta H_{cal}) - (M_{3,d,h}\Delta h_{3,d,h} + M_w\Delta h_{3,w} + M_{18,s,a}\Delta h_{18,s,a} + M_{15,p,a}\Delta h_{15,p,a})$$

Based on the stoichiometry of the combustion chemical reaction of methane (equation 4) for the conventional calcination process, the masses of each secondary (combustion) air and

exhaust gases are expressed as a function of the mass flow rate of fuel $M_f = M_{22,CH_4}$ as follows and substituted in the equation 30. The mass of secondary (combustion) air at the calciner inlet is expressed based on the stoichiometry of the NG combustion reaction:

$$M_{18,s,a} = 2\left(\frac{MW_{O_2}}{MW_{CH_4}} + 3.72\frac{MW_{N_2}}{MW_{CH_4}}\right) \times M_{22,CH_4} \tag{28}$$

The total mass flow rate of exhaust gases exiting the calciner (produced by calcination reaction 2 and combustion reaction 4) is the sum of the mass flow rates of N_2, CO_2, H_2O and primary air:

$$M_{19,g} = M_{19,p,a} + M_{19,H_2O,cal} + M_{19,H_2O,comb} + M_{19,CO_2} + M_{19,N_2}$$

$$= M_{19,p,a} + M_{19,H_2O,cal} + \left(2\,\frac{MW_{H_2O}}{MW_{CH_4}} \times M_{22,CH_4}\right) + \left(\frac{MW_{CO_2}}{MW_{CH_4}} \times M_{22,CH_4}\right) + \left(7.52\,\frac{MW_{N_2}}{MW_{CH_4}} \times M_{22,CH_4}\right) \tag{29}$$

Equation (26) is then re-arranged using equations (28) and (29) into the following form to calculate the mass flow rate of the combustion fuel (NG) for calcination:

$$Mf = M_{22,CH_4} = \frac{(M_{19,p,a}\Delta h_{19,p,a} + M_{19,H_2O,cal}\,\Delta h_{19,H_2O} + M_{4,ala}\Delta h_{4,ala} + M_w H_{vap} + \Delta H_{cal}) - (M_{3,d,h}\Delta h_{3,d,h} + M_w\Delta h_{3,w} + M_{15,p,a}\Delta h_{15,p,a})}{(\Delta h_{22,CH_4} + LHV_{CH_4}) + \frac{1}{MW_{CH_4}}(2MW_{O_2}\Delta h_{18,O_2} + 7.52MW_{N_2}\Delta h_{18,N_2} - MW_{CO_2}\Delta h_{19,CO_2} - 2MW_{H_2O}\Delta h_{19,H_2O,comb} - 7.52MW_{N_2}\Delta h_{19,N_2})} \tag{30}$$

The specific thermal energy consumption (SEC) of the calciner is then found using equation (27). The consumption of methane (CH4) is found to be 0.1079-ton CH_4/tAl, therefore based on methane calorific value (50 MJ/kg CH_4) the SEC for conventional calciner is found to be 5.3959 GJ/tAl (2.8329 GJ/tAla) using equation (27).

Using the same methodology, the mass of low-carbon hydrogen and the thermal SEC of the PtH_2 calciner per ton of aluminum are estimated. The mass of secondary (combustion air) at the calciner inlet is expressed based on the stoichiometry of the H_2 combustion reaction:

$$M_{18,s,a,H_2} = 0.5\left(\frac{MW_{O_2}}{MW_{H_2}} + 3.72\frac{MW_{N_2}}{MW_{H_2}}\right) \times M_{22,H_2} \tag{31}$$

The total mass flow rate of exhaust gases (produced by calcination reaction 2 and combustion reaction 3) exiting the calciner is the sum of the mass flow rates of N_2, H_2O and primary air:

$$M_{19,g,H_2} = M_{19,p,a} + M_{19,H_2O,cal} + M_{19,H_2O,comb} + M_{19,N_2}$$

$$= M_{19,p,a} + M_{19,H_2O,cal} + \left(2\,\frac{MW_{H_2O}}{MW_{H_2}} \times M_{22,H_2}\right) + \left(1.88\,\frac{MW_{N_2}}{MW_{H_2}} \times M_{22,H_2}\right) \tag{32}$$

Equation (26) is then re-arranged using equations (31) and (32) into the following form (33) to calculate the mass flow rate of the combustion fuel (H_2) for calcination:

$$Mf = M_{22,H_2} = \frac{(M_{19,p,a}\Delta h_{19,p,a} + M_{19,H_2O,cal}\,\Delta h_{19,H_2O} + M_{4,ala}\Delta h_{4,ala} + M_w H_{vap} + \Delta H_{cal}) - (M_{3,d,h}\Delta h_{3,d,h} + M_w \Delta h_{3,w} + M_{15,p,a}\Delta h_{15,p,a})}{(\Delta h_{22,H_2} + LHV_{H_2}) + \frac{1}{MW_{H_2}}(0.5MW_{O_2}\Delta h_{18,O_2} + 1.88MW_{N_2}\Delta h_{18,N_2} - MW_{H_2O}\Delta h_{19,H_2O} - 1.88MW_{N_2}\Delta h_{19,N_2})} \quad (33)$$

The calculated mass of hydrogen supplied to the calciner per ton of aluminum produced is 0.0443 ton/tAl. The specific thermal energy consumption for the PtH_2 calciner is found to be slightly lower 5.3462 GJ/tAl (2.8068 GJ/tAla) than for NG. This is due to combination of differences in mass flow rate of entering fuel, entering secondary air, and exiting gases, as well as the inlet temperature of hydrogen (70°C) versus NG (ambient, 25°C).

5.2.2 Hall-Heroult process

Only consumable materials (alumina, carbon anode, carbon dioxide and aluminum) have been considered for this calculation. The cryolite utilized in the bath, for example, has not been taken into account because it cannot be consumed during the reduction (or is lost in a very small portion). As carbon dioxide emissions constitute the largest proportion of emissions from the reduction process, only these emissions are taken into account.

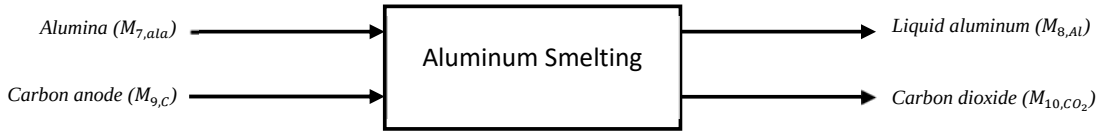


Fig. 12 Aluminum reduction in the Hall–Heroult process. The output products are assumed to have the same temperature as the reduction temperature of 950°C.

Applying the principle of energy conservation to the reacting systems is necessary to calculate the theoretical energy needs. Figure 12 depicts the net reaction for the carbon anode Hall-Heroult process, while equation (34) summarizes the theoretical energy requirement as shown below.

$$SEC_{theor,Al,ele} = \left(M_{8,Al}\Delta h_{8,Al} + M_{10,CO_2}\Delta h_{10,CO_2} + \Delta H_{Al,elect}\right) - \left(M_{7,ala}\Delta h_{7,ala} + M_{9,C}\Delta h_{9,C}\right) \quad (34)$$

$$= [(1 \times 1.0129) + (1.6308 \times 1.0403) + (20.11)] - [(1.9105 \times 0.0474) + (0.45 \times 0)]$$

$$= 22.7288\ \frac{GJ}{t\ Al} = 6.3136\ \frac{MWh}{t\ Al}$$

All values to be calculated corresponding to 1 ton of aluminum. Therefore, the total theoretical minimum energy requirement for the Hall–Heroult process is $6.3136 \frac{MWh}{t\ Al}$. The actual electrical consumption of the Hall–Heroult reduction process, $SEC_{Al,elect}$, can be determined by the following relation [91][92].

$$SEC_{Al,elect} = \frac{298 \times V_{cell}}{CE} \tag{35}$$

where $SEC_{Al,elect}$ is in (MWh/t Al), V_{cell} is the aluminum cell's total voltage in V. The typical total voltage for the current Hall–Heroult cells is 4.2 V [91][93], and CE is the cell's current efficiency as a percentage. Briefly, CE is current efficiency and in most modern cells is above 90% [91][92]. A maximum of 95–98.5% current efficiency has reportedly been reached by the best-equipped smelters [69][93][94]. Therefore, the typical electrical consumption of the current Hall–Heroult cell with 96% current efficiency is $SEC_{Al,elect}$= 14.0301 MWh/t Al. The Hall-Heroult process efficiency, $\eta_{Hall-Hauralt}$ can be estimated as:

$$\eta_{Hall-Hauralt} = \frac{\text{Theoretical electrical requirement}}{\text{Actual electrical requirement}} = \frac{6.3136}{14.0301} = 0.45 \tag{36}$$

5.2.3 Low-temperature water electrolysis plant

The low carbon hydrogen is produced through LTE with an efficiency of 80% [53]. The specific energy consumption is evaluated depending on the higher heating value of the hydrogen.

$$SEC_{LTE} = \frac{\text{HHV}_{H_2}}{\eta_{LTE}} = \frac{141.7}{0.8} = 177.1250\ \frac{MJ}{kg\ H_2} = 4.9649\ \frac{GJ}{t\ Al} \tag{37}$$

The hydrogen produced is directed to the calciner furnace with an inlet temperature of 70°C which is the operating temperature of water electrolysis.

6. Results and Discussion

The total energy, and carbon emission modeling results obtained for both the conventional NG-based calciner and PtH_2 calciner - alumina electrolyser are shown in Table 7. In addition, calculated stream properties for the NG-based conventional and PtH_2 calcination-alumina electrolysis processes are presented in Tables 4 and 5 respectively.

6.1 Comparison of Modeling Results with Literature Values for the Conventional Calcination and Smelting Process

Mass, temperature, specific energy consumption (SEC) and emission for conventional production of 1 ton of liquid aluminum have been compared with the results available in the literature, shown in Table 6. The predicted SEC of the conventional NG-based calcination process is found to be 5.3959 GJ/tAl (2.8329 GJ/tAla), given the enthalpies as an input value, which is similar to the previously reported for NG calciner processes analysed in steady conditions in a range from 2.79-2.9 GJ/tAla [22][23][69][96][100]. Many factors that can affect the SEC of calcination are the type of ore material, temperatures, and the efficiency of the calciner furnace.

The SEC of alumina electrolysis is the same for both designs, 14.0302 MWh_e/t Al, that is 50.5085 GJ/tAl, and is in line with previously reported values (11–16 MWh/t Al) [67][68][69][93]. The total conventional NG-based model direct emission intensity is of 2.1369 tCO_2/tAl, including 0.296 tCO_2/tAl from fuel combustion in the calcination process, which is in line with the reported value in a previous study (0.28 tCO_2/t Al [69]). Direct process emissions from carbon anode consumption during alumina electrolysis are 1.6308 tCO_2/tAl (compared with 1.53 tCO_2/tAl [11], 1.4-1.7 [76], 1.66 tCO_2/tAl [92]). Additional emissions, not calculated by the model, would occur from anode baking (0.21 tCO_2/tAl [11]).

Table 6. Comparison of present conventional process model predictions with corresponding reference data.

Parameter	This work	Literature values
Masses		
Mass of alumina hydrate (t/tAl)	2.2685	2.28[76]
Mass of alumina (t/tAl)	1.9047	1.92 (1.9-1.93) [29][31][58][67][76][106]
Mass of carbon anode (t/tAl)	0.4452	0.43 (0.4-0.45) [29][31][58][76][106]
Temperatures		
Alumina outlet temperature from direct cooling stages (°C)	330.25	330[67]
Temperature of preheated secondary air entering the calciner (°C)	644.75	525[107]
Outlet temperature of primary air exiting the FBC (°C)	102.4353	153[107]
Energy		
Specific thermal energy consumption of conventional calciner (natural gas calorific value) (GJ/tAla)	2.8329	2.84 (2.79 -2.9) [22][23][69][96][100]
Equivalent to (GJ/tAl)	5.3959	5.4094
Heat loss from produced alumina to the primary air and water in the calciner plant alumina fluid bed cooling system (MJ/tAl) (equation 18)	511.6385	419.035[67]
Specific thermal electricity consumption of aluminum electrolysis (smelter) (MWh/tAl)	14.0301	14 (11-16) [67][68][69][93]
Equivalent to (GJ/tAl)	50.5085	50.4
Emissions		
Direct emission from fuel combustion in conventional calciner (t/tAl)	0.2960	0.28[69]
Direct process emissions from anode decomposition in the aluminum smelting process (t/tAl), excluding anode baking	1.6308	1.6 [11][51][76][92]

6.2 Comparison of Energy Consumption and Emissions for the Conventional and PtH_2-based Processes

As summarized in Section 5.2.1, the predicted SEC for the integrated H_2 calciner stands at 5.3462 GJ/tAl (or 2.8068 GJ/tAla), which is slightly lower (by 49.7 MJ/tAl) compared to the conventional NG calciner. The total and distribution of energy consumption for the combined calcination and smelting process is presented in Table 7, both for the conventional NG and the H_2-based processes. Because of the LTE efficiency assumption, the electricity consumption for H_2 production is slightly higher than the chemical/thermal energy requirement of the conventional calcination process. The LTE electrolysis consumption leads to a higher total electricity requirement for the H_2-based process (58.8876 GJ/tAl) compared with the conventional NG process (51.0388 GJ/tAl).

The overall emission intensity for the PtH_2 calciner and alumina electrolyser process is 2.06 tCO_2/tAl, which is lower than the emission intensity of the conventional NG process at 2.2775 tCO_2/tAl, by a difference of 217.6 $kgCO_2$/tAl, for the same electricity emission factor assumed (10 gCO_2/kWh_e). The calcination emission intensity decreased due to CO_2-free combustion using hydrogen (H_2) instead of natural gas (NG) during the calcination process, resulting in

reduced direct process emissions. By implementing this change, direct process emissions are reduced from 296 $kgCO_2/tAl$ for the NG process to approximately zero, thereby contributing to a more environmentally friendly process. This reduction is primarily attributed to the electricity emissions for hydrogen production being lower than methane combustion emissions for the electricity emission factor assumed.

Table 7. Main technical energy and emission intensity modeling results for the overall calciner and alumina electrolyser processes, including calcination furnace fuel input/production, calciner air blowers and ESP, smelting electricity, smelter anode baking, anodic carbon consumed in smelting, and Al ingot casting (considered as fuel) at base case operating conditions. Ingot casting emissions are not included. Digestion, clarification, and precipitation (GJ/tAl) energy requirement (16.65[76]) and emissions are not included.

Parameter		
	NG-based process	H_2-based process
Energy		
Chemical/thermal energy		
NG fuel for calcination (GJ/tAl)	5.3959	-
Carbon anode inlet energy for aluminum smelting - coal HHV (GJ/tAl)	14-15.37[29][76]	14-15.37[29][76]
Anode baking (GJ/tAl)	2.66[76]	2.66[76]
Ingot casting (GJ/tAl)	1.6[29]	1.6[29]
Sub-total	23.6559-25.0259	18.26-19.63
Electricity		
LTE (GJ_e/tAl)	-	7.8488
Air blowers and ESP for calcination (GJ_e/tAl)	0.1303	0.1303
Aluminum electrolysis (smelting) (GJ_e/tAl)	50.5085	50.5085
Ingot casting (GJ_e/tAl)	0.4[29]	0.4[29]
Sub-total (GJ_e/tAl)	51.0388	58.8876
Total energy consumption	74.6947-76.0647	77.1476-78.5176
Selected emissions		
Process emissions		
Direct combustion process emissions from calcination (tCO_2/tAl)	0.2960	0
Direct process emissions from anode carbon consumption (tCO_2/tAl)	1.6308	1.6308
Direct process emissions from anode baking (tCO_2/tAl)	0.21[11]	0.21[11]
Sub-total	2.1369	1.8408
Electricity emissions*		
LTE (tCO_2/tAl)	0	0.0785
Aluminum Smelting (tCO_2/tAl)	0.1403	0.1403
Air blowers and ESP (tCO_2/tAl)	0.00036	0.00036
Sub-total	0.2192	0.1407
Total system's emissions	2.2775	2.0600

*The grid emission factor of 10 gCO_2/kWh_e as an example.

6.3 Emissions in different Countries

In this section, the environmental impact of transitioning to a hydrogen-based calciner in major aluminum-producing countries is assessed. Specifically, the focus is on the United Arab Emirates (UAE), Saudi Arabia (SA), and Germany, which are large Al producers and are considered solar-rich nations and potential candidates for establishing on-site PV (photovoltaic) plants in future steps. The analysis is based on grid emission factors reported for the year 2020, as documented in reference [60], with values of (0.4041, 0.5059, 0.5374,

0.33866, 0.00567, 0.00762 kgCO_2/kWh) for UAE, Saudi Arabia, China (largest aluminum producer), Germany, Sweden, and Norway respectively. The results of the assessment are illustrated in Figure 13. Globally, hydropower (used in EU countries mostly) contributes approximately 15% of the total energy used in aluminum production, as per the International Energy Agency (IEA) 2022 report [43] Although it used to be much more significant, accounted for 40% of the total energy used in aluminum production in 2010 compared to 30% in 2021. This reduction in hydropower contribution to aluminum production is primarily due to increased aluminum production in China, where coal still dominates and supplies 80% of the electricity used in manufacturing [43].

As a result, China exhibits the highest potential for CO_2 emissions among the selected countries, with an estimated total of approximately 10.5717 tCO_2/tAl for PtH_2 alumina and aluminum production (indirect emissions from electricity usage of each air blowers/ESP, H_2 production, and smelting, in addition to direct emission of anode consumption from aluminum smelting and anode baking), with ~83% of these emissions being indirect electricity emissions for smelting, LTE and air blowing/ESP. Saudi Arabia follows closely as the second-highest potential emitter, at 8.2192 tCO_2/tAl of indirect emissions compared to China. This is primarily due to Saudi Arabia's heavy reliance on fossil fuels for electricity production, with 65% sourced from natural gas and 35% from oil [78].

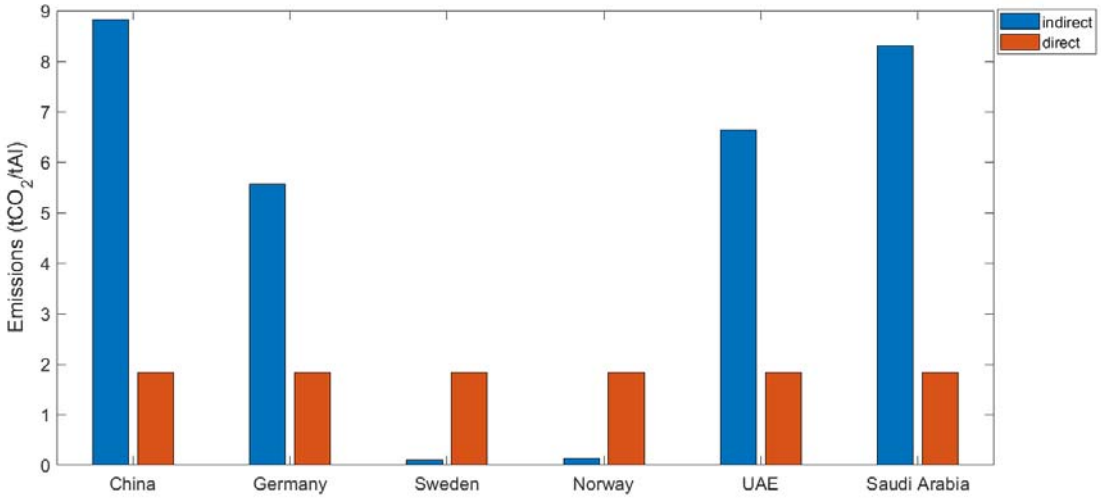


Fig. 13 Carbon intensity of the PtH_2 calcination-electrolysis model in different selected countries. (Note electricity emission factors for year 2020: 0.4041, 0.5059, 0.5374, 0.33866, 0.00567, 0.00762 kgCO_2/kWh) for UAE, Saudi Arabia, China, Germany, Sweden, and Norway respectively). These countries are responsible for 3.83%, 1.53%, 57.15%, 2.75%, 0.2%, and 2% of global aluminum production in year 2020. Emissions represented are indirect emissions from electricity usage of each air blowers/ESP, H_2 production, and smelting, in addition to direct emission of anode consumption and anode baking.

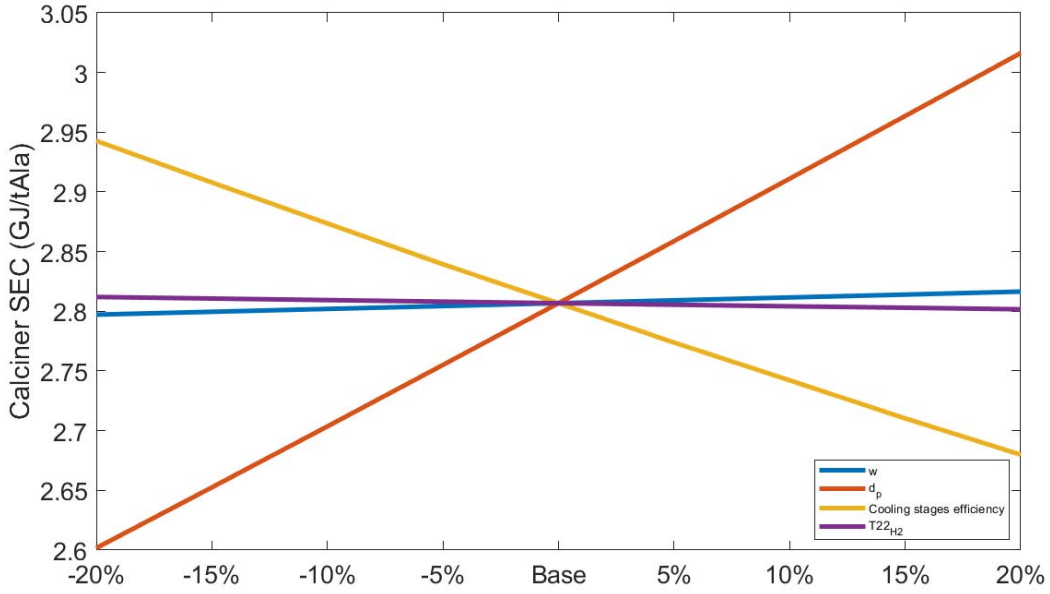
The UAE shows an estimated 6.5653 tCO_2/tAl of indirect emissions because it primarily uses natural gas for electricity generation, considered a clean fossil fuel option [79]. In contrast, in Europe, North America, and South America, hydroelectric power accounts for over 75% of electricity used in aluminum production. Consequently, Norway and Sweden have the lowest indirect CO_2 emissions, with values of 0.1238 and 0.0921 tCO_2/tAl, respectively. The next step in the analysis will focus on further reducing influential emission in regions with insufficient hydro power by utilizing on-site PV electricity.

6.4 Sensitivity Analysis

A sensitivity analysis was performed to assess how sensitive the model outputs are to changes or perturbations in its input parameters. This analysis was conducted by individually varying input parameters one at a time by ±5%, ±10%, ±15%, and ±20%, while keeping the other parameters constant. The parameters subjected to sensitivity analysis include moisture content of hydrate (w), CFB furnace particle diameter (d_p), heat transfer efficiency of direct cooling stages (η_c), hydrogen temperature (T_{22,H_2}) at the calciner inlet, LTE electrolyser efficiency (η_{LTE}), and the electricity emission factor. The goal was to understand their impact on both the calciner SEC and total emissions. The outcomes of this sensitivity analysis are represented in Figure 14 and Figure 15.

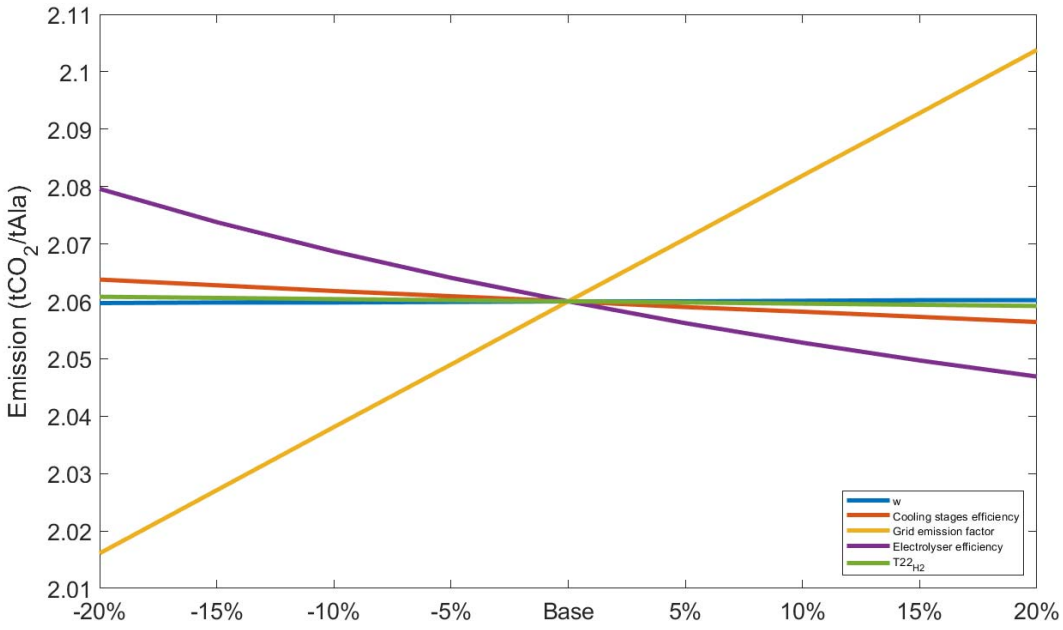
The results indicate that the CFB furnace particle diameter has the most significant impact on the calciner's SEC. This is because the primary air mass flow rate is closely tied to particle diameter, as explained in section 5.1.1.2. One important factor affecting calciner energy consumption is the efficiency of the direct cooling stages. For the base case, an efficiency of 67% is used as reported in Raahauge [67]. Increasing the efficiency significantly reduces energy consumption.

Emissions from the system are primarily linked to the electricity emission factor. The electrolyser efficiency is another crucial factor that directly impacts overall emissions from the system because it is directly related to its electricity consumption. As electrolyser efficiency increases, emissions decrease. In contrast, hydrogen input temperature and hydrate moisture content have minimal effects on calciner energy requirements and emissions in the PtH_2 calcination-electrolysis system. This suggests that hydrogen pre-heating (e.g., electrically) would not be effective and can increase indirect emissions when implemented.



Note: w =water content of alumina hydrate (base = 6 wt%, 4.8 – 7.2 wt%), d_p= calciner average particle diameter (base = 250 µm, 200 – 300 µm), η_c = overall efficiency of cooling stages efficiency (base = 67%, 53.6 – 80.4), T_{22,H_2} = hydrogen temperature at calciner inlet (base = 343.15 K, 274.4 – 411.6 K)

Fig. 14 Sensitivity analysis of H_2 calciner process SEC to identify the parameters that influence the specific energy requirements of the calciner.



Note: w =water content of alumina hydrate (base = 6 wt%, 4.8 – 7.2 wt%), d_p= calciner average particle diameter (base = 250 µm, 200 – 300 µm), η_c = overall efficiency of cooling stages efficiency (base = 67%, 53.6 – 80.4%), T_{22,H_2} = hydrogen temperature at calciner inlet (base = 343.15 K, 274.4 – 411.6 K), η_{LTE} = LTE efficiency (base = 80% , 64 – 96%), grid emission factor (base = 0.01 $kgCO_2/kWh$, 0.008 – 0.012 $kgCO_2/kWh$).

Fig. 15 Sensitivity analysis to identify the key parameters that have the most significant impact on the CO_2 emissions generated by the PtH_2 calcination-electrolysis systems.

A parametric analysis was conducted to assess the considerable impact of the grid emission factor on the overall emissions of calcination-electrolysis systems, both for NG-based and H_2-based calciners, covering a range from 0 to 0.4 $kgCO_2/kWh$. Figure 16 illustrates that the emissions from H_2-based calcination-electrolysis systems are lower than those from NG-based systems when the emission factor is roughly below 0.04 $kgCO_2/kWh$. However, if the emission factor exceeds this threshold, the emissions from H_2-based system significantly surpass those from conventional system. Utilizing renewable energy sources for electricity generation stands out as the most effective means to reduce indirect emissions as discussed in section 2.2.1. In Figure 16, there is a composite renewable energy emission factor for reference. It includes values for wind, nuclear, hydropower, and solar energy at 0.008, 0.015, 0.024, and 0.04 $kgCO_2/kWh$, respectively. Notably, when these renewable energy sources are employed, the total emissions from H_2-based system are lower than those from NG-based system.

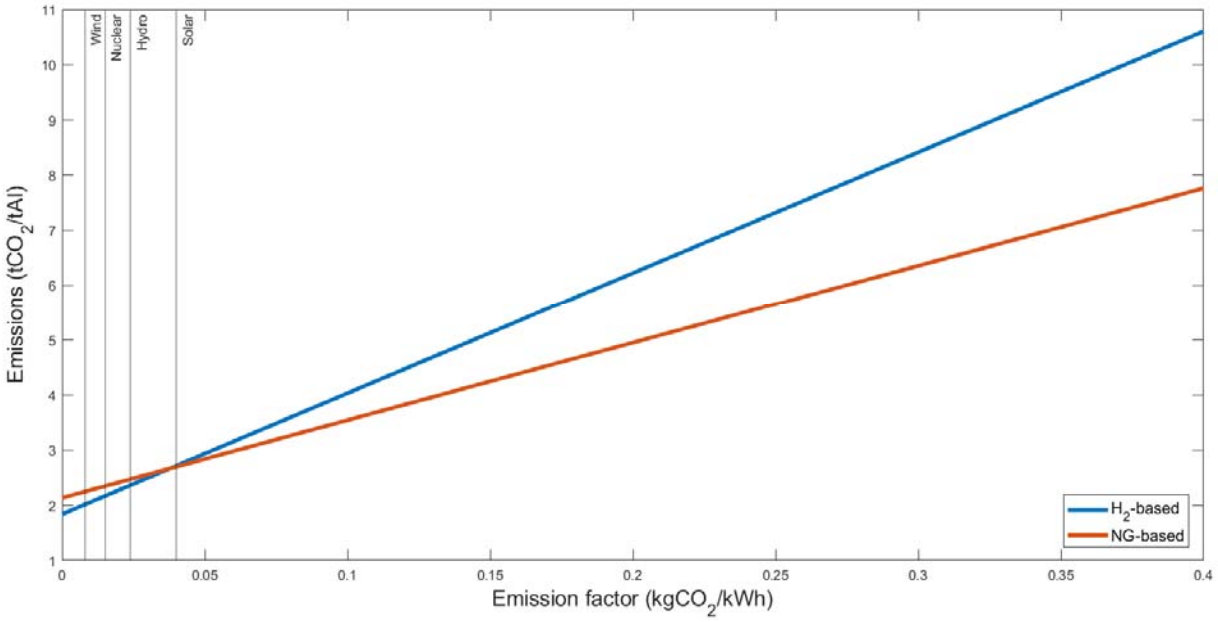


Fig. 16 Parametric analysis to study the effect of the electricity source emission factor on the total emissions of both the NG- and the H_2-based calcination-electrolysis systems.

7. Conclusions and Recommendations

The energy consumption and emission intensity, of PtH_2 calcination and alumina electrolysis processes, were investigated and compared with those of a conventional NG-based process, with the main objective to improve the environmental and economic competitiveness of the aluminum industry.

7.1 Conclusions

Based on the obtained results, using a hydrogen fueled calciner could reduce the direct emission intensity of the calcination process by 0.296 tCO_2/tAl (13.8% of total system emissions) when compared to a typical conventional natural gas calciner, at an electricity emission factor of 10 gCO_2/kWh_e.

In parallel, indirect emissions from electricity production for smelting, water electrolysis and air blower/ESP are reduced from 0.2192 tCO_2/tAl for the conventional process to approximately 0.1407 tCO_2/tAl. An electricity emission factor of 40 gCO_2/kWh_e or lower is required to reduce total emissions compared to the conventional system. Transitioning to a low-carbon aluminum sector will therefore require significant amounts of low-carbon electricity.

The sensitivity analysis also highlights the importance of calciner cooling stages efficiency on calciner energy consumption.

7.2 Recommendations

The following future work packages are recommended:

- Investigation of calciner design/retrofitting and optimum conditions for operation on hydrogen, including via detailed kinetic modeling of the calcination process.
- Evaluation of other emissions such as NO_x.
- Dynamic modeling of hydrogen-based calcination using variable renewable electricity sources (e.g., solar PV in UAE).
- Cost analysis of hydrogen-based calcination in comparison with NG-based calcination.

8. References

[1] The Paris Agreement. United Nations - Climate Change. Retrieved March 9, 2022, Available: https://unfccc.int/process-and-meetings/the-paris-agreement/the-paris-agreement

[2] Re-thinking 2050: a 100% renewable energy vision for European Union. (2010). European Renewable Energy Council. Retrieved March 10, 2022, Available: https://warwick.ac.uk/fac/soc/pais/research/researchcentres/csgr/green/foresight/energyenvironment/2010_erec_rethinkhing_2050.pdf

[3] Krausmann, F., Gingrich, S., Eisenmenger, N., Erb, K., Haberl, H., & Fischer-Kowalski, M. (2009). Growth in global materials use, GDP and population during the 20th century. Ecological Economics, 68(10), 2696–2705.

[4] IEA (2010). CO_2 Emissions from Fuel Combustion. International Energy Agency, Paris, France, p.512.

[5] Allwood, J. M., Cullen, J. M., & Milford, R. L. (2010). Options for achieving a 50% cut in industrial carbon emissions by 2050. Environmental Science & Technology 44(6), 1888-1894.

[6] Jouhara, H., & Olabi, A. G. (2018). Editorial: Industrial waste heat recovery. Energy, 160(1–2), https://doi-org.libconnect.ku.ac.ae/10.1016/j.energy.2018.07.013

[7] Agathokleous, R. A., Bianchi, G., Panayiotou, G., Aresti, L., Argyrou, M. C., Georgiou, G. S., Tassou, S. A., Jouhara, H., Kalogirou, S. A., Florides, G. A., & Christodoulides, P. (2019). Waste Heat Recovery in the EU industry and proposed new technologies. Energy Procedia, 161, 489–496, https://doi.org/10.1016/j.egypro.2019.02.064

[8] Brown, T.J. Idoine, N.E. Raycraft, E.R. Shaw, R.A. Hobbs, S.F. Everett, P. et al., (2018). World Mineral Production 2012-2016, British Geological Survey. https://www2.bgs.ac.uk/mineralsuk/download/world_statistics/2010s/WMP_2012_2016.pdf

[9] Schlesinger, M.E.. Aluminum Recycling: Second Edition. Aluminum Recycling: Second Edition, 1 January 2013, :1-263 Language: English. CRC Press DOI: 10.1201/b16192

[10] Liu, G., & Müller, D. B. (2012). Addressing sustainability in the aluminum industry: a critical review of life cycle assessments. Journal of Cleaner Production, 35, 108–117, https://doi.org/10.1016/j.jclepro.2012.05.030

[11] Saevarsdottir, G., Kvande, H., & Welch, B. J. (2020). Aluminum Production in the Times of Climate Change: The Global Challenge to Reduce the Carbon Footprint and Prevent Carbon Leakage. JOM: The Journal of The Minerals, Metals & Materials Society (TMS), 72(1), 296–308, https://doi-org.libconnect.ku.ac.ae/10.1007/s11837-019-03918-6

[12] Kermeli, K., Weer, P.H., Crijns-Graus, W., Worrell, E., 2015. Energy efficiency improvement and GHG abatement in the global production of primary aluminum. Energy Effic. 8 (4), 629e666m https://doi.org/10.1007/s12053-014-9301-7

[13] Das, S., 2012. Achieving carbon neutrality in the global aluminum industry. JOM 64 (2), 285e290, https://doi.org/10.1007/s11837-012-0237-0

[14] Menzie, W. D., Barry, J., Bleiwas, D. I., Bray, E. L., Goonan, T. G., & Matos, G. R. (2010). The global flow of aluminum from 2006 through 2025. Open-file Report, https://doi.org/10.3133/ofr20101256

[15] Das, S. (2012). Achieving Carbon Neutrality in the Global Aluminum Industry. JOM, 64(2), 285–290, https://doi-org.libconnect.ku.ac.ae/10.1007/s11837-012-0237-0.

[16] Luo, Z., & Soria, A. (2007). Prospective study of the world aluminium industry. JRC Scientific and Technical Reports, EUR, 22951, ftp://ftp.jrc.es/pub/EURdoc/JRC40221.pdf

[17] World Aluminium, Current IAI Statistics (2019), Available: https://www.world-aluminium.org/statistics/primary-aluminium-smelting-energy-intensity/#data.

[18] Steinfeld A. (1997). High-temperature solar thermochemistry for CO_2 mitigation in the extractive metallurgical industry, Energy 22, 311–316, doi: 10.1016/S0360-5442(96)00103-X.

[19] IAI (2021), Aluminium Sector Greenhouse Gas Pathways to 2050, Available: https://international-aluminium.org/resource/aluminium-sector-greenhouse-gas-pathways-to-2050-2021/

[20] Tabereaux, A. T., & Peterson, R. D. (2014). Aluminum production. In Elsevier eBooks (pp. 839–917), https://doi.org/10.1016/b978-0-08-096988-6.00023-7

[21] Lumley, R. (2011). Fundamentals of aluminium metallurgy. [electronic resource]: production, processing and applications. Woodhead.

[22] Perander, L.M., Gasafi, E., Scarsella, A., (2018). Cost and Energy Efficiency Improvement in Alumina Calcination, Alumina Quality Workshop Inc., https://www.aqw.com.au/papers/category/2018

[23] Klett, C., Reeb, B., Missalla, M., Schmidt, HW. (2011). Methods to Reduce Operating Costs in Circulating Fluidized Bed Calcination. In: Lindsay, S.J. (eds) Light Metals 2011. Springer, Cham., https://doi.org/10.1007/978-3-319-48160-9_22

[24] Raahauge, B.E., Devarajan, N. (2015). Experience with Particle Breakdown in Gas Suspension Calciners, Presented at the International Committee for the Study of Bauxite, Alumina and Aluminium (ICSOBA) Conference, UAE, Dubai.

[25] Nowicki, C., & Gosselin, L. (2012). An overview of opportunities for waste heat recovery and thermal integration in the primary aluminum industry. JOM, 64(8), 990–996, https://doi.org/10.1007/s11837-012-0367-4.

[26] Johnson, I., Choate, W.T., & Davidson, A. (2008). Waste heat recovery: technology opportunities in the US Industry, US Dep. Energy Ind. Technol. Progr 1–112.

[27] Haraldsson, J., & Johansson, M. T. (2018). Review of measures for improved energy efficiency in production-related processes in the aluminium industry - From electrolysis to recycling. Renewable & Sustainable Energy Reviews, 93, 525–548, https://doi-org.libconnect.ku.ac.ae/10.1016/j.rser.2018.05.043

[28] Aluminium production process-Bayer & Hall-Héroult. (2012), Available: http://processflowsheets.blogspot.com/2012/05/aluminium-production-processbayer-hall.html

[29] Moya, J. A., Boulamati, A., Slingerland, S., van der Veen, R., Gancheva, M., Rademaekers, K. M., & Visschedijk, A. J. H. (2015). Energy Efficiency and GHG Emissions: Prospective Scenarios for the Aluminium Industry, http://trinomics.eu/wp-content/uploads/2015/02/ldna27335enn.pdf

[30] Fischer, C., Fox, A.K. (2012). Comparing policies to combat emissions leakage: border carbon adjustments versus rebates. J. Environ. Econ. Management. 64,199-216, https://doi.org/10.1016/j.jeem.2012.01.005.

[31] IEA (2020), Global CO_2 emissions in 2019, IEA, Paris. Available: https://international-aluminium.org/statistics/greenhouse-gas-emissions-intensity-primary-aluminium/

[32] IRENA (2021), Renewable Power Generation Costs in 2021. Available: https://www.irena.org/publications/2022/Jul/Renewable-Power-Generation-Costs-in-2021

[33] UN Environment Programme (2019), Emissions Gap Report 2019. Available: https://wedocs.unep.org/bitstream/handle/20.500.11822/30798/EGR19ESEN.pdf

[34] Evans, S. and Gabbatiss, J., (2020). Solar Is Now 'Cheapest Electricity in History', Confirms IEA, Carbon Brief, doi: https://www.carbonbrief.org/solar-is-now-cheapest-electricity-in-history-confirms-iea

[35] Aluminium Insider, (2020). China Hongqiao Begins Production at Hydroelectricity-Powered Aluminium Smelter in Yunnan, https://aluminiuminsider.com/china-hongqiao-begins-production-at-hydroelectricity-poweredaluminium-smelter-in-yunnan/

[36] Executive Summary of the Vision 2050 Report. European Aluminium. Available: https://www.european-aluminium.eu/vision2050/#:~:text=A%20vision%20for%20strategic%2C%20low%20carbon%20and%20competitive%20aluminium&text=This%20is%20in%20line%20with,by%202050%20compared%20to%201990

[37] Aluminium for Climate: Exploring pathways to decarbonize the aluminium industry, (2020). Available: https://www3.weforum.org/docs/WEF_Aluminium_for_Climate_2020.pdf

[38] Davis, D., Müller, F., Steinfeld, A., & Nathan, G. J. (2017). Solar-driven alumina calcination for CO_2 mitigation and improved product quality. Green Chemistry, 19(13), 2992–3005, https://doi.org/10.1039/c7gc00585g

[39] Meier, A., Bonaldi, E., Cella, G. M., Lipiński, W., Wuillemin, D., & Palumbo, R. (2004). Design and experimental investigation of a horizontal rotary reactor for the solar thermal production of lime. Energy, 29(5–6), 811–821, https://doi.org/10.1016/s0360-5442(03)00187-7

[40] Nikulshina, V., Halmann, M., & Steinfeld, A. (2009). Coproduction of Syngas and lime by combined CACO3-Calcination and CH4-Reforming using a Particle-Flow reactor driven by concentrated solar radiation. Energy & Fuels, 23(12), 6207–6212, https://doi.org/10.1021/ef9007246

[41] Rio Tinto plans to adopt renewable hydrogen for decarbonizing alumina refining. (2022, March 15). Alcircle, https://www.alcircle.com/news/rio-tinto-plans-to-adopt-renewable-hydrogen-for-decarbonizing-alumina-refining-77841

[42] Worcester-Bosch, Hydrogen-fired boiler, (2020), Available: https://www.worcester-bosch.co.uk/hydrogen

[43] IEA, Aluminium, 2020. Available: https://www.iea.org/reports/aluminium

[44] European Aluminium Statistics based on global trade atlas. (2009). Available: https://www.european-aluminium.eu/data/recycling-data/recycling-eu-net-exports-of-aluminium-scrap/

[45] Light Metal Age, Novelis Creates Automotive Closed-Loop Recycling System with Volvo Cars, (2020), https://www.lightmetalage.com/news/industry-news/recycling-remelt/novelis-creates-automotive-closed-loop-recyclingsystem-with-volvo-cars

[46] Sterner, M. (2009). Bioenergy and Renewable Power Methane in Integrated 100% Renewable Energy Systems: Limiting Global Warming by Transforming Energy Systems 14, Kassel university press GmbH, http://publica.fraunhofer.de/documents/N-139644.html

[47] Greener aluminium - Air Products (2021), Can hydrogen and the latest burners reduce carbon emissions. Available: https://www.airproducts.com/-/media/airproducts/files/external/aluminium-international-today/greener-alu-air-products.pdf

[48] IEA (2020), Renewables. IEA, Paris. Available: https://www.iea.org/fuels-and-technologies/renewables

[49] IRENA (2018), "Hydrogen from renewable power", International Renewable Energy Agency, Abu Dhabi, Available:www.irena.org/-/media/Files/IRENA/Agency/Publication/2018/Sep/IRENA_ Hydrogen_from_renewable_power_2018.pdf

[50] Smolinka, T., Günther, M., & Garche, J. (2011). Stand und Entwicklungspotenzial der Wasserelektrolyse zur Herstellung von Wasserstoff aus regenerativen Energien. Available: http://www.hs-ansbach.de/uploads/tx_nxlinks/NOW-Studie-Wasserelektrolyse-2011.pdf

[51] IEA ETSAP. (2012). Aluminium Production. www.etsap.org. Accessed 23 Feb 2022.

[52] Lindsay, S. J., & Welch, B. J. (2021). A Review: Understanding the Science and the Impacts of Impurities upon the Electrolytic Bath of Hall–Héroult Reduction Cells. JOM, 73(4), 1196–1209, https://doi.org/10.1007/s11837-021-04572-7

[53] Lettenmeier, P. (2021). White paper l Efficiency – Electrolysis. Siemens Energy. Retrieved March 18, 2023, https://assets.siemens-energy.com/siemens/assets/api/uuid:a33a8c39-b694-4d91-a0b5-4d8c9464e96c/efficiency-white-paper.pdf

[54] D. Panias, I. Paspaliaris, (2003). Boehmite Process – A New Approach in Alumina Production, World of Metallurgy - ERZMETALL, vol. 56, pp. 75-81

[55] Alumina Hydrate | NALCO (National Aluminium Company Limited) | A Govt. of India Enterprise, https://nalcoindia.com/business/products/alumina-hydrate/alumina-hydrate/

[56] Calcined Alumina | NALCO (National Aluminium Company Limited) | A Govt. of India Enterprise, https://nalcoindia.com/business/products/alumina-hydrate/calcined-alumina/

[57] Curtolo, D. C., Xiong, N., Friedrich, S., & Friedrich, B. (2021). High- and Ultra-High-Purity Aluminum, A review on technical production methodologies. Metals, 11(9), 1407, https://doi.org/10.3390/met11091407

[58] Kvande, H., & Drabløs, P. A. (2014). The aluminum smelting process and innovative alternative technologies. Journal of Occupational and Environmental Medicine, 56(Supplement 5S), S23–S32, https://doi.org/10.1097/jom.0000000000000062

[59] Bhandaru, S. H. 38th conference and exhibition ICSOBA 2020 – ICSOBA, https://icsoba.org/proceedings/38th-conference-and-exibition-icsoba-2020/?doc=27

[60] Country Specific Electricity Grid Greenhouse Gas Emission Factors. (2022b, March). Carbon Footprint. Retrieved November 20, 2022, https://www.carbonfootprint.com/docs/2022_03_emissions_factors_sources_for_2021_electricity_v11.pdf

[61] Neuwirth, M., Fleiter, T., Manz, P., & Hofmann, R. (2022). The future potential hydrogen demand in energy-intensive industries - a site-specific approach applied to Germany. Energy Conversion and Management, 252, 115052, https://doi.org/10.1016/j.enconman.2021.115052

[62] Aulakh, D. J. S., Boulama, K. G., & Pharoah, J. G. (2021). On the reduction of electric energy consumption in electrolysis: A thermodynamic study. International Journal of Hydrogen Energy, 46(33), 17084–17096, https://doi.org/10.1016/j.ijhydene.2021.02.161

[63] Robie, R. A., & David R. W. (2000). Thermodynamic Properties of Minerals and Related Substances at 298.15 K (25°C) and 1 Atmosphere (1.013 Bars) Pressure and At Higher Temperatures.

[64] NIST-JANAF Thermochemical Tables. Available: https://janaf.nist.gov/

[65] Robie, R. A., & Bruch S. H. (1995). Thermodynamic properties of minerals and related substances at 298.15 K and 1 bar (10[5] pascals) pressure and at higher temperatures.

[66] National Institute of Standards and Technology.v*Methane*, https://webbook.nist.gov/cgi/cbook.cgi?ID=C74828&Mask=1#Thermo-Gas

[67] Raahauge, B.E. (2022). Production of Smelter Grade Alumina (SGA) by Calcination. Smelter Grade Alumina from Bauxite. Springer Series in Materials Science, vol 320. Springer, Cham. https://doi.org/10.1007/978-3-030-88586-1_10

[68] ITP, Feasibility Study of CST Technologies for the Low Temperature Requirements of the Bayer Alumina Process, https://www.adelaide.edu.au/cet/solar-alumina/ua/media/75/ITP%20Alumina%20Report%20Public%2030112020.pdf

[69] Brough, D., & Jouhara, H. (2020). The aluminium industry: A review on state-of-the-art technologies, environmental impacts and possibilities for waste heat recovery. International Journal of Thermofluids, 1–2.

[70] National Institute of Standards and Technology. Water, https://webbook.nist.gov/cgi/cbook.cgi?ID=C7732185

[71] National Institute of Standards and Technology. Hydrogen, https://webbook.nist.gov/cgi/cbook.cgi?ID=C1333740

[72] National Institute of Standards and Technology. *Carbon dioxide*, https://webbook.nist.gov/cgi/cbook.cgi?ID=C124389

[73] National Institute of Standards and Technology. A*luminium hydroxide oxide*, https://webbook.nist.gov/cgi/cbook.cgi?Name=aluminium+hydroxide+oxide

[74] National Institute of Standards and Technology. A*luminium oxide*, https://webbook.nist.gov/cgi/cbook.cgi?ID=C1344281

[75] National Institute of Standards and Technology. Aluminum, https://webbook.nist.gov/cgi/cbook.cgi?ID=C7429905

[76] Balomenos, E., Panias, D., & Paspaliaris, I. (2011). Energy and Exergy Analysis of the Primary Aluminum Production Processes: A Review on Current and Future Sustainability. *Mineral Processing and Extractive Metallurgy Review*, *32*(2), 69–89, https://doi.org/10.1080/08827508.2010.530721

[77] Fuels - Higher and Lower Calorific Values, https://www.engineeringtoolbox.com/fuels-higher-calorific-values-d_169.html

[78] Climate Transparency Report Comparing G20 Climate Action And Responses To The Covid-19 Crisis. (2020). Climate Transparency, https://www.climate-transparency.org/wp-content/uploads/2020/11/Saudi-Arabia-CT-2020.pdf

[79] Electricity - The Official Portal of the UAE Government. (2022, November), https://u.ae/en/information-and-services/environment-and-energy/water-and-energy/electricity

[80] European Commission, JR Science for Policy Report: Best Available Techniques (BAT) Reference Document for the Non-Ferrous Metals Industries, (2017). Available: https://eippcb.jrc.ec.europa.eu/sites/default/files/2020-01/JRC107041_ NFM_bref2017.pdf

[81] Yu, Miao, (2018). Waste Heat Recovery from Aluminium Production, Reykjavik University. Available: https://skemman.is/bitstream/1946/29774/1/Miao_Waste%20Heat%20Recovery%20from%20Aluminum%20Production.pdf

[82] Eglinton, T., Hinkley, J., Beath, A., & Dell'Amico, M. (2013). Potential Applications of Concentrated Solar Thermal Technologies in the Australian Minerals Processing and Extractive Metallurgical Industry. JOM, 65(12), 1710–1720, https://doi-org.libconnect.ku.ac.ae/10.1007/s11837-013-0707-z

[83] Eurometaux, (2019). Metals for a Climate Neutral Europe: A 2050 Blueprint. Available: https://eurometaux.eu/metals-blueprint-2050/

[84] Mission Possible Partnership, (2021). Closing The Gap For Aluminium Emissions: Technologies to Accelerate Deep Decarbonization of Direct Emissions. Available: https://missionpossiblepartnership.org/wp-content/uploads/2021/12/Closing-the-Gap-for-Aluminium-Emissions.pdf

[85] The Future of Hydrogen: Seizing Today's Opportunities, OECD, Paris Cedex 16, https://doi.org/10.1787/1e0514c4-en

[86] EnPot, How EnPot Works, Available: https://www.energiapotior.com/ how-enpot-works.

[87] REEL International, Environmental Control Solutions. Available: https://www.reelinternational.com/en/industries/ aluminum/environmental-control-solutions/

[88] Cronus Technology, Make It Sustainable. Available: https://www. cronustechnology.no/sustainability-in-aluminium.

[89] Spector, J., (2019). CSP Startup Heliogen Cranks Up Solar Thermal to 1,000 Degrees, Green Tech Media. Available: https://www.greentechmedia.com/articles/read/heliogen-cranks-solar-thermal-up-to-1000-degrees-cel

[90] Special and Chemical Grade Alumina Calcination Plant - Metso Outotec. Metso Outotec, https://www.mogroup.com/portfolio/special-and-chemical-grade-alumina-calcination-plant/

[91] Mohammad, I., (2023). On Stabilizing Aluminium Electrolysis Cells with Oscillating Currents. University of Rochester, http://hajim.rochester.edu/me/sites/kelley/papers/MohammadDissertation.pdf

[92] Obaidat, M., Al-Ghandoor, A., Phelan, P. E., Villalobos, R., & Alkhalidi, A. (2018b). Energy and Exergy Analyses of Different Aluminum Reduction Technologies. Sustainability, 10(4), 1216, https://doi.org/10.3390/su10041216

[93] Tabereaux, A. T. (2018, November 30). Production of Primary Aluminum by Electrolysis, https://doi.org/10.31399/asm.hb.v02a.a0006483

[94] Prasad, S. (2000). Studies on the Hall-Heroult aluminum electrowinning process. Journal of the Brazilian Chemical Society, 11(3), 245–251, https://doi.org/10.1590/s0103-50532000000300008

[95] Making Net-Zero Aluminium Possible. (2022). The Mission Possible Partnership, https://missionpossiblepartnership.org/wp-content/uploads/2022/10/Making-1.5-Aligned-Aluminium-possible.pdf

[96] Klett, I. C., Missalla, M., Bligh, R., Stroeder, I. M., Hiltunen, P., & Graham, M. (2007). Outokumpu Technology's State-of-the-Art CFB Calciners – A Review. European Metallurgical Conference (EMC).

[97] Samani, N. A. (2020). Calcination in an electrically heated bubbling fluidized bed applied in calcium looping. USN. Retrieved May 16, 2023, https://hdl.handle.net/11250/2724254

[98] Freij, S.J. and G.M. Parkinson, Surface morphology and crystal growth mechanism of gibbsite in industrial Bayer liquors. Hydrometallurgy, 2005, 78(3-4): p. 246-255.

[99] Amiri, A., Ingram, G. D., Maynard, N., Livk, I., & Bekker, A. (2010). A Multi-scale Modelling Outlook for Gibbsite Calcination. Chemeca 2010: Engineering at the Edge; 26-29 September 2010, Hilton Adelaide, South Australia, 1187, https://espace.curtin.edu.au/handle/20.500.11937/31243

[100] Klett, C., & Perander, L. (2015). Alumina Calcination: A Mature Technology Under Review from Supplier Perspective. In Light Metal 2015, https://doi.org/10.1007/978-3-319-48248-4_15

[101] Reh, L., Schmidt, H.W. (2016). Application of Circulating Fluid Bed Calciners in Large-size Alumina Plants. In: Donaldson, D., Raahauge, B.E. (eds) Essential Readings in Light Metals. Springer, Cham., https://doi.org/10.1007/978-3-319-48176-0_89

[102] Kvande, H. (2011). Production of primary aluminium. In Elsevier eBooks (pp.49–69), https://doi.org/10.1533/9780857090256.1.49

[103] Edge, E. Viscosity of air, dynamic and kinematic, https://www.engineersedge.com/physics/viscosity_of_air_dynamic_and_kinematic_14483.htm#:~:text=The%20viscosity%20of%20air%20depends,2%20%2Fs%20or%2014.8%20cSt.

[104] Barthelmy, D. Boehmite Mineral Data, http://webmineral.com/data/Boehmite.shtml

[105] Water - Heat of Vaporization vs. Temperature, https://www.engineeringtoolbox.com/water-properties-d_1573.html?vA=25&units=C#

[106] Worrell, E. (2007, June 5). World Best Practice Energy Intensity Values for selected industrial sectors. https://escholarship.org/uc/item/77n9d4sp

[107] Schmidt, H. W. (1995, November 14). US6015539A - Fluidized bed process for producing alumina from aluminum hydroxide - Google Patents, https://patents.google.com/patent/US6015539A/en

[108] Deng, L., Johnson, S. E., & Gençer, E. (2022). Environmental-Techno-Economic analysis of decarbonization strategies for the Indian aluminum industry. Energy Conversion and Management, 274, 116455, https://doi.org/10.1016/j.enconman.2022.116455

[109] Ndjebayi, J. N. (2017). Aluminum Production Costs: A Comparative Case Study of Production Strategy. Walden Dissertations and Doctoral Studies Collection, https://scholarworks.waldenu.edu/cgi/viewcontent.cgi?article=5571&context=dissertations

[110] Reh, L., Schmidt, H.W. (2016). Application of Circulating Fluid Bed Calciners in Large-size Alumina Plants. In: Donaldson, D., Raahauge, B.E. (eds). Essential Readings in Light Metals. Springer, Cham., https://doi.org/10.1007/978-3-319-48176-0_89

[111] Perander, L.M., et al. (2011). Two perspectives on the evolution and future of alumina, in Light Metals, pp. 151–155.

Appendix I

Table A1. Coefficients of Shomate Equation for each substance in given temperature range relevant to this analysis.

	(Al_2O_3 · H_2O) [73]	**Al_2O_3 [74]**	**Al [75]**	**H_2O [70]**	**H_2O [70]**	**CO_2 [72]**	**CH_4 [66]**	**H_2 [71]**
Temperature (K)	298. - 6000.	298. - 2327.	933.45 - 2790.812	500. - 1700.	298. - 500.	298. - 1200.	298. - 1300.	298. - 1000.
A	60.80733	108.6830	31.75104	30.09200	-203.6060	24.99735	-0.703029	33.066178
B	15.18466	37.22630	3.935826×10^{-8}	6.832514	1523.290	55.18696	108.4773	-11.363417
C	-3.608529	-14.20650	-1.786515×10^{-8}	6.793435	-3196.413	-33.69137	-42.52157	11.432816
D	0.283720	2.193601	2.694171×10^{-9}	-2.534480	2474.455	7.948387	5.862788	-2.772874
E	-1.407093	-3.209881	5.480037×10^{-9}	0.082139	3.855326	-0.136638	0.678565	-0.158558
F	-483.7332	-1701.600	-0.945684	-250.8810	-256.5478	-403.6075	-76.84376	-9.980797
G	315.4535	155.1360	73.39949	223.3967	-488.7163	228.2431	158.7163	172.707974
H	-460.2400	-1656.860	10.56201	-241.8264	-285.8304	-393.5224	-74.87310	0.0